Acta Mech 224, 41–61 (2013)
DOI 10.1007/s00707-012-0741-x

Changyong Cao · Aibing Yu · Qing-Hua Qin

A new hybrid finite element approach for plane piezoelectricity with defects

Received: 7 June 2012 / Revised: 5 September 2012 / Published online: 13 October 2012

Abstract In this paper, a new type of hybrid fundamental solution-based finite element method (HFS-FEM) is developed for analyzing plane piezoelectric problems with defects by employing fundamental solutions (or Green's functions) as internal interpolation functions. The hybrid method is formulated based on two independent assumptions: an intra-element field covering the element domain and an inter-element frame field along the element boundary. Both general elements and a special element with a central elliptical hole or crack are developed in this work. The fundamental solutions of piezoelectricity derived from the elegant Stroh formalism are employed to approximate the intra-element displacement field of the elements, while the polynomial shape functions used in traditional FEM are utilized to interpolate the frame field. By using Stroh formalism, the computation and implementation of the method are considerably simplified in comparison with methods using Lekhnitskii's formalism. The special-purpose hole element developed in this work can be used efficiently to model defects such as voids or cracks embedded in piezoelectric materials. Numerical examples are presented to assess the performance of the new method by comparing it with analytical or numerical results from the literature.

1 Introduction

Piezoelectric materials have the property of converting electrical energy into mechanical energy and vice versa. This reciprocity in energy conversion makes them very attractive for applications in electromechanical devices such as sensors, actuators, transducers, and frequency generators. It has been demonstrated that the presence of defects such as voids and cracks results in degeneration of the service performance of piezoelectric materials [1,2]. An analysis of electroelastic fields around defects in piezoelectric materials is of paramount importance for evaluating the failure behavior of such materials. To understand the electromechanical coupling mechanism of piezoelectric materials, much research has been conducted over recent decades, both analytically and numerically [3–10]. Because analytical solutions can only be obtained for problems with simple geometry and boundary conditions, numerical methods such as the finite element method (FEM) and boundary element method (BEM) are employed in solving most practical problems [11,12].

It should be mentioned that mesh refinement near a hole or crack is required for FEM to achieve meaningful results, which is a very time-consuming and complex task [13]. Compared with the FEM, the BEM is computationally efficient and highly accurate in dealing with linear fracture analyses. Lee and Jiang [14] developed a boundary element formulation for piezoelectric solids using the method of weighted residuals. Pan [15]

C. Cao · Q.-H. Qin (✉)
Research School of Engineering, Australian National University, Canberra, ACT 0200, Australia
E-mail: Qinghua.qin@anu.edu.au

A. Yu
School of Materials Science and Engineering, University of New South Wales, Sydney, NSW 2052, Australia

presented a boundary element model for analyzing the fracture behavior in two-dimensional anisotropic piezoelectric solids based on the Green's functions derived by Stroh's formalism. Xu and Rajapakse [16] performed a BEM analysis of crack problems based on Green's functions derived by Lekhnitskii formalism. Sheng et al. [17] developed a multi-domain Trefftz boundary collocation method for plane piezoelectricity with defects according to the plane piezoelectricity solution derived by Lekhnitskii formalism. To avoid mesh refinement, special Green's functions for two-dimensional anisotropic and piezoelectric materials were proposed in [18,19] and a linear boundary element was developed to analyze problems involving multiple holes and cracks by utilizing special Green's functions [19,20]. In the present work, a special Green's function for an infinite piezoelectric body containing an elliptic hole is employed to satisfy, a priori, the proper singularity at the source point and the traction-free-hole boundary conditions along the rim of the elliptic hole, rendering meshing refinement around the hole boundary unnecessary. Thus, a vast amount of computer time and storage for numerical calculations can be saved. Moreover, due to the exact satisfaction of the traction-free-hole boundary condition, the results are more accurate than those obtained using conventional boundary elements [20].

On the other hand, during the past three decades, the Hybrid-Trefftz finite element method (HT-FEM) has been considerably improved and has now become a highly efficient computational tool for the solution of complex boundary value problems [21–24]. The concept of special-purpose functions has been found to be highly efficient for dealing with various geometry or load-dependent singularities and local effects such as obtuse or reentrant corners, cracks, circular or elliptic holes, and concentrated loads [7,25–27]. However, special attention must be given to the derivation and selection of a truncated T-complete solution set for HT-FEM to ensure that the completeness of solutions is retained and the corresponding rigid-body motion terms are discarded to avoid singularity during the process of matrix inversion. Furthermore, to ensure good numerical condition during the inversion of the matrix **H**, a coordinate transformation is usually required, because the order of coordinates or distance variables will increase along with an increase in the terms of T-complete solutions. Recently, a novel hybrid finite element formulation, called HFS-FEM, was developed based on the framework of HT-FEM [28–31]. In this new method, the major improvement over the HT-FEM is the use of the linear combination of fundamental solutions for modeling the intra-element field. The fundamental solution employed satisfies analytically the related governing equation. The resulting system of equations from the modified hybrid variational functional is expressed in terms of a symmetric stiffness matrix and nodal displacements only, which is easy to implement into the standard FEM. It is noted that, by locating the source point outside the element of interest to avoid overlapping with any field point during the computation, no singular integrals are involved in the HFS-FEM [28].

The proposed HFS-FEM inherits all the advantages of HT-FEM over the traditional FEM and the BEM, namely domain decomposition and boundary integral expressions, while avoiding the major weaknesses of BEM, namely the singular element boundary integral and loss of symmetry and sparsity [3]. The employment of two independent fields also makes it easier for the HFS-FEM to use arbitrary polygonal or even curve-sided elements. It also obviates the difficulties that occur in HT-FEM [27] in deriving T-complete functions for certain complex or new physical problems [27]. The HFS-FEM has simpler interpolation kernel expressions for intra-element fields (fundamental solutions) and avoids the coordinate transformation procedure required in the HT-FEM to keep the matrix inversion stable. Moreover, this approach also has the potential to achieve high accuracy using coarse meshes of high-degree elements, enhancing insensitivity to mesh distortion, which allows great liberty in element shape and accurate representation of various local effects (such as hole, crack, and inclusions) without troublesome mesh adjustment [7,26].

In this paper, a new hybrid fundamental solution-based FEM is developed for modeling plane piezoelectricity with defects (holes or cracks) based on extended Stroh formalism [6]. The fundamental solution expressed in the form of the extended Stroh formalism is employed to approximate the intra-element displacement and electrical potential field (DEP). A new modified variational functional is proposed to facilitate the implement of the HFS-FEM for piezoelectric materials. This new scheme is much simpler and more elegant than that based on Lekhnitskii formalism for transversely isotropic piezoelectric materials [3]. It is demonstrated from numerical examples that the new HFS-FEM is capable of analyzing the coupling behavior of piezoelectric materials and structures. More importantly, a special-purpose element for handling problems with elliptic holes is proposed.

This paper is organized as follows: in Sect. 2, the basic equations and the extended Stroh formalism for plane piezoelectricity are presented. The fundamental solutions for a normal element and a special-purpose hole element are presented by the way of Stroh formalism. Section 3 presents detailed formulations of the HFS-FEM for plane piezoelectricity, including the establishment of a modified variational functional and element stiffness matrix. In Sect. 4, the HFS-FEM is assessed by four numerical examples in

which comparisons are made with results from the literature. Concluding remarks are briefly presented in Sect. 5.

2 Basic equations and Stroh formalism for piezoelectric materials

2.1 Basic equations

In the Cartesian coordinate system (x_1, x_2, x_3), the differential governing equations for a linear piezoelectric material are given by

$$\sigma_{ij,j} + f_i = 0, \quad D_{i,i} - q = 0 \quad \text{in } \Omega, \tag{1}$$

where σ_{ij} is the stress tensor, D_i the electric displacement vector, f_i the body force, q the free charge densities, and Ω the solution domain. The subscript comma denotes the partial differentiation with respect to the coordinates after the comma. The summation convention is invoked over repeated indices.

With strain ε_{ij} and electric field E_i as the independent variables, the constitutive equations are

$$\sigma_{ij} = C_{ijkl}\varepsilon_{kl} - e_{kij}E_k, \quad D_i = e_{ikl}\varepsilon_{kl} + \kappa_{ik}E_k, \tag{2}$$

where C_{ijkl} is the elasticity tensor measured under constant electric field ($E = 0$), e_{ikl} and κ_{ij} are, respectively, the piezoelectric tensor and dielectric tensor measured under constant strain ($\varepsilon = 0$). The strain–displacement and electric field–electric potential relations are given as

$$\varepsilon_{ij} = \frac{1}{2}(u_{i,j} + u_{j,i}), \quad E_i = -\phi_{,i}, \tag{3}$$

where u_i and ϕ are the displacement and the electric potential, respectively.

The boundary conditions of the boundary value problem (1)–(3) are given by

$$u_i = \overline{u_i} \quad \text{on } \Gamma_u, \tag{4}$$

$$t_i = \sigma_{ij}n_j = \overline{t_i} \quad \text{on } \Gamma_t, \tag{5}$$

$$\phi = \overline{\phi} \quad \text{on } \Gamma_\phi, \tag{6}$$

$$D_n = D_i n_i = -\overline{q} \quad \text{on } \Gamma_D, \tag{7}$$

where t_i is the traction, q is the surface charge, and n_i is the unit outward normal vector. A bar over a variable indicates that its value is prescribed. $\Gamma = \Gamma_u + \Gamma_t = \Gamma_D + \Gamma_\phi$ is the boundary of the problem domain Ω.

2.2 Extended Stroh formalism

If we neglect the body force f_i and surface charge q and let [18]

$$C_{IJKL} = \begin{cases} C_{ijkl} & i, j, k, l = 1, 2, 3, \\ e_{lij} & k = 4,\ i, j, l = 1, 2, 3, \\ e_{jkl} & i = 4,\ j, k, l = 1, 2, 3, \\ -\kappa_{jl} & i = k = 4,\ j, l = 1, 2, 3, \end{cases} \tag{8}$$

$$D_j = \sigma_{4j}, \quad -E_j = u_{4,j} = 2\varepsilon_{4j}, \quad j = 1, 2, 3, \tag{9}$$

the basic equations (1)–(3) can be expressed in terms of expanded tensor notation by

$$\sigma_{IJ,J} = 0, \quad \sigma_{IJ} = C_{IJKL}\varepsilon_{KL}, \quad \varepsilon_{IJ} = \frac{1}{2}(u_{I,J} + u_{J,I}), \quad I, J, K, L = 1, 2, 3, 4, \tag{10}$$

where C_{IJKL} has the following symmetry property:

$$C_{IJKL} = C_{JIKL} = C_{IJLK} = C_{KLIJ}. \tag{11}$$

It is noted that the governing equations (10) and (11) for piezoelectric anisotropic materials have the same form as those of pure anisotropic elasticity. For the generalized two-dimensional deformation (u_i depends on

x_1 and x_2 only), an extended version of Stroh formalism satisfying the governing Eq. (10) was proposed by Kuo and Barnett as [18,32]

$$\mathbf{u} = 2\mathrm{Re}\{\mathbf{A}\mathbf{f}(z)\}, \boldsymbol{\varphi} = 2\mathrm{Re}\{\mathbf{B}\mathbf{f}(z)\}, \tag{12}$$

where $\mathbf{u} = [u_1, u_2, u_3, \phi]^{\mathrm{T}}$ is the displacement vector, $\boldsymbol{\varphi} = [\varphi_1, \varphi_2, \varphi_3, \varphi_4]^{\mathrm{T}}$ is the stress function vector, $\mathbf{f}(z) = [f_1(z_1), f_2(z_2), f_3(z_3), f_4(z_4)]^{\mathrm{T}}$ is a function vector composed of four holomorphic complex functions $f_\alpha(z_\alpha), \alpha = 1, 2, 3, 4$, which is an arbitrary function with argument $z_\alpha = x_1 + p_\alpha x_2$ and will be determined by satisfying the boundary and loading conditions of a given problem. In Eq. (12), Re stands for the real part of a complex number, p_α are the material eigenvalues with positive imaginary part, $\mathbf{A} = \left[\mathbf{a_1}, \mathbf{a_2}, \mathbf{a_3}, \mathbf{a_4}\right]$ and $\mathbf{B} = [\mathbf{b_1}, \mathbf{b_2}, \mathbf{b_3}, \mathbf{b_4}]$ are 4×4 complex matrices formed by the material eigenvector associated with p_α, which can be obtained by the following eigen relations [18]:

$$\mathbf{N}\boldsymbol{\xi} = p\boldsymbol{\xi}, \tag{13}$$

where $\mathbf{N}$ is an 8×8 fundamental elasticity matrix and $\boldsymbol{\xi}$ is an 8×1 column vector defined by

$$\mathbf{N} = \begin{bmatrix} \mathbf{N}_1 & \mathbf{N}_2 \\ \mathbf{N}_3 & \mathbf{N}_1^{\mathbf{T}} \end{bmatrix}, \ \boldsymbol{\xi} = \begin{Bmatrix} \mathbf{a} \\ \mathbf{b} \end{Bmatrix}, \tag{14}$$

where $\mathbf{N_1} = -\mathbf{T}^{-\mathbf{1}}\mathbf{R}^{\mathbf{T}}$, $\mathbf{N_2} = \mathbf{T}^{-\mathbf{1}} = \mathbf{N_2^T}$, $\mathbf{N_3} = \mathbf{R}\mathbf{T}^{-\mathbf{1}}\mathbf{R}^{\mathbf{T}} - \mathbf{Q} = \mathbf{N_3^T}$, and the matrices $\mathbf{Q}$, $\mathbf{R}$ and $\mathbf{T}$ are 4×4 matrices extracted from C_{IJKL} as follows:

$$Q_{ik} = C_{i1k1}, R_{ik} = C_{i1k2}, T_{ik} = C_{i2k2} \qquad i, k = 1, 2, 3, 4; \tag{15}$$

the detailed matrix components are shown below as

$$\mathbf{Q} = \begin{bmatrix} C_{11} & C_{16} & C_{15} & e_{11} \\ C_{16} & C_{66} & C_{56} & e_{16} \\ C_{15} & C_{56} & C_{55} & e_{15} \\ e_{11} & e_{16} & e_{15} & -k_{11} \end{bmatrix}, \mathbf{R} = \begin{bmatrix} C_{16} & C_{12} & C_{14} & e_{21} \\ C_{66} & C_{26} & C_{46} & e_{26} \\ C_{56} & C_{25} & C_{45} & e_{25} \\ e_{16} & e_{12} & e_{14} & -k_{12} \end{bmatrix}, \mathbf{T} = \begin{bmatrix} C_{66} & C_{26} & C_{46} & e_{26} \\ C_{26} & C_{22} & C_{24} & e_{22} \\ C_{46} & C_{24} & C_{44} & e_{24} \\ e_{26} & e_{22} & e_{24} & -k_{22} \end{bmatrix}. \tag{16}$$

Since $\boldsymbol{\xi} = [\mathbf{a}, \mathbf{b}]^{\mathrm{T}}$ is the right eigenvector of matrix $\mathbf{N}$, normalization is necessary to obtain unique values of $\mathbf{a}_k$ and $\mathbf{b}_k$. As in anisotropic elasticity, the following orthogonality relation for material eigenvector matrices $\mathbf{A}$ and $\mathbf{B}$ can be used for this purpose:

$$\begin{bmatrix} \mathbf{A} & \overline{\mathbf{A}} \\ \mathbf{B} & \overline{\mathbf{B}} \end{bmatrix} \begin{bmatrix} \mathbf{B}^{\mathbf{T}} & \mathbf{A}^{\mathbf{T}} \\ \overline{\mathbf{B}}^{\mathbf{T}} & \overline{\mathbf{A}}^{\mathbf{T}} \end{bmatrix} = \begin{bmatrix} \mathbf{I} & \mathbf{0} \\ \mathbf{0} & \mathbf{I} \end{bmatrix}. \tag{17}$$

It should be noted that when using transversely piezoelectric materials (e.g., x_1–x_2 as the isotropic plane), and taking the x_3 as the poling direction, Stroh formalism will fail for such degenerate materials, namely $\mu_1 = \mu_2 = \mu_3 = \mu_4 = i$. In this case, a small perturbation must be added to enable the Stroh formalism to work. Based on the relation in Eq. (17), the Barnett–Lothe tensors $\mathbf{L}$, $\mathbf{S}$ and $\mathbf{H}$ can be defined by [18]

$$\mathbf{H} = i\mathbf{2}\mathbf{A}\mathbf{A}^{\mathbf{T}}, \ \mathbf{L} = -i\mathbf{2}\mathbf{B}\mathbf{B}^{\mathbf{T}}, \ \mathbf{S} = i(\mathbf{2}\mathbf{A}\mathbf{B}^{\mathbf{T}} - \mathbf{I}). \tag{18}$$

The stresses and electric displacement can be obtained from the derivation of the generalized stress function $\boldsymbol{\varphi}$ as follows:

$$\sigma_{i1} = -\phi_{i,2}, \quad \sigma_{i2} = \phi_{i,1}, \quad i = 1, 2, 3, \tag{19}$$

$$\sigma_{41} = D_1 = -\phi_{4,2}, \quad \sigma, _{42} = D_2 = \phi_{4,1}. \tag{20}$$

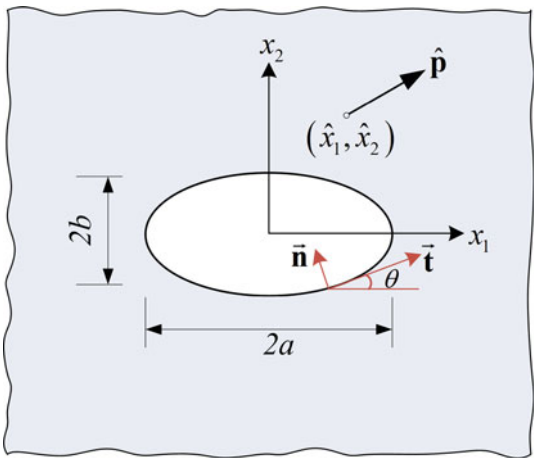

Fig. 1 Schematic of an infinite anisotropic plate with an elliptical hole

2.3 Fundamental solutions

The fundamental solution employed in this work can be found in [18]. To provide an introduction to the solution and notation for later sections, we here summarize briefly the derivation given in [18]. Consider an infinite homogeneous piezoelectric medium loaded by a concentrated point force or electric charge $\hat{\mathbf{p}} = (\hat{p}_1, \hat{p}_2, \hat{p}_3, \hat{p}_4)$ applied at an internal point $\hat{\mathbf{x}} = (\hat{x}_1, \hat{x}_2)$ distant from the boundary. The boundary conditions of this problem can be written as

$$\begin{aligned} &\int_C \mathrm{d}\boldsymbol{\phi} = \hat{\mathbf{p}} \qquad \text{for any closed curve } C \text{ enclosing } \hat{\mathbf{x}}, \\ &\int_C \mathrm{d}\mathbf{u} = \hat{\mathbf{p}} \qquad \text{for any closed curve } C, \\ &\lim_{\mathbf{x}\to\infty} \sigma_{ij} = 0, \ \lim_{\mathbf{x}\to\infty} D_i = 0. \end{aligned} \tag{21}$$

The function f in Eq. (12) satisfying the above boundary conditions has been found to be [18]

$$f(z) = \frac{1}{2\pi i}\langle \ln(z_\alpha - \hat{z}_\alpha)\rangle \mathbf{A}^{\mathrm{T}}\hat{\mathbf{p}}. \tag{22}$$

Therefore, the fundamental solutions of the problem can be expressed as

$$\begin{aligned} \mathbf{u} &= \frac{1}{\pi}\mathrm{Im}\left\{\mathbf{A}\langle \ln\left(z_\alpha - \hat{z}_\alpha\right)\rangle \mathbf{A}^{\mathbf{T}}\right\}\hat{\mathbf{p}}, \\ \phi &= \frac{1}{\pi}\mathrm{Im}\left\{\mathbf{B}\langle \ln\left(z_\alpha - \hat{z}_\alpha\right)\rangle \mathbf{A}^{\mathbf{T}}\right\}\hat{\mathbf{p}}. \end{aligned} \tag{23}$$

The corresponding stress components can be obtained from stress function ϕ as

$$\begin{aligned} \sigma_{i1}^{*} &= -\phi_{,2} = -\frac{1}{\pi}\mathrm{Im}\left\{\mathbf{B}\langle p_\alpha/\left(z_\alpha - \hat{z}_\alpha\right)\rangle \mathbf{A}^{\mathbf{T}}\right\}\hat{\mathbf{p}}, \\ \sigma_{i2}^{*} &= \phi_{,1} = \frac{1}{\pi}\mathrm{Im}\left\{\mathbf{B}\langle 1/\left(z_\alpha - \hat{z}_\alpha\right)\rangle \mathbf{A}^{\mathbf{T}}\right\}\hat{\mathbf{p}}, \end{aligned} \tag{24}$$

where $\hat{\mathbf{p}}$ is chosen to be $(1, 0, 0, 0)^{\mathrm{T}}$, $(0, 1, 0, 0)^{\mathrm{T}}$, $(0, 0, 1, 0)^{\mathrm{T}}$, and $(0, 0, 0, 1)^{\mathrm{T}}$, respectively, $\langle\cdot_\alpha\rangle$ stands for the diagonal matrix corresponding to subscript α, Im denotes the imaginary part of a complex number, and superscript T denotes the matrix transpose.

2.4 Special fundamental solutions for a plate with hole

Consider an infinite anisotropic plate containing traction and an electric-charge-free elliptic hole under a concentrated force or electric charge $\hat{\mathbf{p}} = (\hat{p}_1, \hat{p}_2, \hat{p}_3, \hat{p}_4)$ applied at point $\hat{\mathbf{x}} = (\hat{x}_1, \hat{x}_2)$, as shown in Fig. 1.

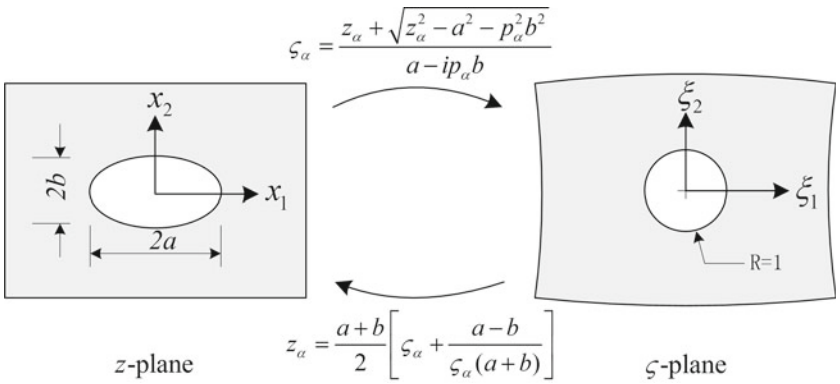

Fig. 2 Conformal mapping of an infinite plane with an elliptical hole

The Green's function of this problem can be obtained by employing the conformal mapping technique as shown in Fig. 2, which transforms the region outside the elliptical hole in the z-plane onto the exterior of a unit circle in the ς-plane. The expressions of the Green's function for this problem have been presented in [18,20] as

$$\begin{aligned}
\mathbf{u} &= \frac{1}{\pi}\mathrm{Im}\left\{\mathbf{A}\left\langle \ln\left(\varsigma_\alpha - \hat{\varsigma}_\alpha\right)\right\rangle \mathbf{A}^{\mathbf{T}} + \sum_{k=1}^{4}\mathbf{A}\left\langle \ln(\varsigma_\alpha^{-1} - \overline{\hat{\varsigma}}_k)\right\rangle \mathbf{B}^{-\mathbf{1}}\overline{\mathbf{B}}\mathbf{I_k}\overline{\mathbf{A}}^{\mathbf{T}}\right\}\hat{\mathbf{p}}, \\
\phi &= \frac{1}{\pi}\mathrm{Im}\left\{\mathbf{B}\ln\left(\varsigma_\alpha - \hat{\varsigma}_\alpha\right)\mathbf{A}^{\mathbf{T}} + \sum_{k=1}^{4}\mathbf{B}\left\langle \ln(\varsigma_\alpha^{-1} - \overline{\hat{\varsigma}}_k)\right\rangle \mathbf{B}^{-\mathbf{1}}\overline{\mathbf{B}}\mathbf{I_k}\overline{\mathbf{A}}^{\mathbf{T}}\right\}\hat{\mathbf{p}},
\end{aligned} \tag{25}$$

in which $\mathbf{I_1} = \mathbf{diag}[1,0,0,0], \mathbf{I}_2 = \mathbf{diag}[0,1,0,0], \mathbf{I}_3 = \mathbf{diag}[0,0,1,0], \mathbf{I}_4 = \mathbf{diag}[0,0,0,1]$, and the variables ς_α and $\hat{\varsigma}_\alpha$ are expressed in terms of the arguments z_α and $\hat{z}_\alpha$ as

$$\varsigma_\alpha = \frac{z_\alpha + \sqrt{z_\alpha^2 - a^2 - p_\alpha^2 b^2}}{a - ip_\alpha b}, \quad \hat{\varsigma}_\alpha = \frac{\hat{z}_\alpha + \sqrt{\hat{z}_\alpha^2 - a^2 - p_\alpha^2 b^2}}{a - ip_\alpha b}, \tag{26}$$

where $2a$ and $2b$ are the lengths of the major and minor axes of the elliptical hole, respectively,

$$z_\alpha = x_1 + p_\alpha x_2, \quad \hat{z}_\alpha = \hat{x}_1 + p_\alpha \hat{x}_2. \tag{27}$$

The derivative of ς_α with respect to z_α can be expressed as

$$\frac{\partial \varsigma_\alpha}{\partial z_\alpha} = \frac{1}{a - ip_\alpha b}\left(1 + \frac{z_\alpha}{\sqrt{z_\alpha^2 - a^2 - p_\alpha^2 b^2}}\right) = \frac{2\varsigma_\alpha^2}{(a - ip_\alpha b)\,\varsigma_\alpha^2 - (a + ip_\alpha b)}. \tag{28}$$

Then, the derivative of ς_α with respect to x_1 and x_2 is given in the form

$$\begin{aligned}
\frac{\partial \varsigma_\alpha}{\partial x_1} &= \frac{\partial \varsigma_\alpha}{\partial z_\alpha}\cdot\frac{\partial z_\alpha}{\partial x_1} = \frac{\partial \varsigma_\alpha}{\partial z_\alpha} = \frac{2\varsigma_\alpha^2}{(a - ip_\alpha b)\,\varsigma_\alpha^2 - (a + ip_\alpha b)}, \\
\frac{\partial \varsigma_\alpha}{\partial x_2} &= \frac{\partial \varsigma_\alpha}{\partial z_\alpha}\cdot\frac{\partial z_\alpha}{\partial x_2} = \frac{\partial \varsigma_\alpha}{\partial z_\alpha}\cdot p_\alpha = \frac{2p_\alpha\varsigma_\alpha^2}{(a - ip_\alpha b)\,\varsigma_\alpha^2 - (a + ip_\alpha b)}.
\end{aligned} \tag{29}$$

Using Eq. (29) and letting $\chi = (a - ip_\alpha b)\varsigma_\alpha^2 - (a + ip_\alpha b)$, the corresponding stress components can be expressed as

$$\begin{aligned}
\sigma_{i1}^* &= -\phi_{,2} = -\frac{1}{\pi}\mathrm{Im}\left\{\mathbf{B}\left\langle \frac{2\varsigma_\alpha^2 p_\alpha}{(\varsigma_\alpha - \hat{\varsigma}_\alpha)\,\chi}\right\rangle \mathbf{A}^{\mathbf{T}}\right\}\hat{\mathbf{p}} - \frac{1}{\pi}\sum_{k=1}^{4}\mathrm{Im}\left\{\mathbf{B}\left\langle \frac{-2\varsigma_\alpha p_\alpha}{\left(1 - \varsigma_\alpha\overline{\hat{\varsigma}}_k\right)\chi}\right\rangle \mathbf{B}^{-\mathbf{1}}\overline{\mathbf{B}}\mathbf{I_k}\overline{\mathbf{A}}^{\mathbf{T}}\right\}\hat{\mathbf{p}}, \\
\sigma_{i2}^* &= \phi_{,1} = \frac{1}{\pi}\mathrm{Im}\left\{\mathbf{B}\left\langle \frac{2\varsigma_\alpha^2}{(\varsigma_\alpha - \hat{\varsigma}_\alpha)\,\chi}\right\rangle \mathbf{A}^{\mathbf{T}}\right\}\hat{\mathbf{p}} + \frac{1}{\pi}\sum_{k=1}^{4}\mathrm{Im}\left\{\mathbf{B}\left\langle \frac{-2\varsigma_\alpha}{\left(1 - \varsigma_\alpha\overline{\hat{\varsigma}}_k\right)\chi}\right\rangle \mathbf{B}^{-\mathbf{1}}\overline{\mathbf{B}}\mathbf{I_k}\overline{\mathbf{A}}^{\mathbf{T}}\right\}\hat{\mathbf{p}}.
\end{aligned} \tag{30}$$

The fundamental solutions for an infinite piezoelectric medium with a crack of length $2a$ can be obtained easily by letting $b = 0$ in Eq. (25) [18]. For crack problems, it is always of interest to know the stress and electric displacement fields near the crack tip. Differentiating the generalized stress function with respect to x_1 and letting $x_2 = 0,\ x_1 > a$, the stress $\boldsymbol{\sigma}_2 = \{\sigma_{21}, \sigma_{22}, \sigma_{23}, D_2\}^{\mathrm{T}}$ ahead of the crack tip along the x_1 axis is obtained as

$$\boldsymbol{\sigma}_2 = \boldsymbol{\varphi}_{,1} = \frac{1}{\pi a}\left(1 + \frac{x_1}{\sqrt{x_1^2 - a^2}}\right) \mathrm{Im}\left\{\mathbf{B}\left\langle \frac{1}{\zeta - \hat{\zeta}_\alpha} + \frac{1}{\zeta - \zeta^2\hat{\zeta}_\alpha}\right\rangle \mathbf{A}^{\mathrm{T}}\right\}\hat{\mathbf{p}} \tag{31}$$

where

$$\zeta = \frac{x_1 + \sqrt{x_1^2 - a^2}}{a},\ \hat{\zeta}_\alpha = \frac{\hat{z}_\alpha + \sqrt{\hat{z}_\alpha^2 - a^2}}{a}. \tag{32}$$

With the definition of stress and the electric displacement intensity factors of cracks [33] and using the following relations:

$$\frac{1}{1 - \hat{\zeta}_\alpha} = \frac{1}{2}\left(1 - \frac{\hat{z}_\alpha + a}{\sqrt{\hat{z}_\alpha^2 - a^2}}\right) = \frac{1}{2}\left(1 + \frac{\sqrt{\hat{z}_\alpha^2 - a^2}}{a - \hat{z}_\alpha}\right),\quad \lim_{x_1 \to a}\zeta = 1, \tag{33}$$

we can obtain

$$K = \begin{Bmatrix} K_{\mathrm{II}} \\ K_{\mathrm{I}} \\ K_{\mathrm{III}} \\ K_{\mathrm{IV}} \end{Bmatrix} = \lim_{x_1 \to a}\sqrt{2\pi(x_1 - a)}\,\boldsymbol{\sigma}_2 = \frac{2}{\sqrt{\pi a}}\mathrm{Im}\left\{\mathbf{B}\left\langle \frac{1}{1 - \hat{\zeta}_\alpha}\right\rangle \mathbf{A}^{\mathrm{T}}\right\}\hat{\mathbf{p}}, \tag{34}$$

where K_{I}, K_{II}, and K_{III} are the stress intensity factors, and K_{IV} is the electric displacement intensity factor [34].

3 Formulations of HFS-FEM for piezoelectricity

3.1 Assumed independent fields

To solve electroelastic problems governed by Eq. (10) using HFS-FEM approach, the solution domain Ω must be divided into a series of elements, as done in the conventional FEM. For each element, two independent DEP fields, that is, the intra-element DEP field and the frame DEP field, are assumed in the manner presented in [28].

3.1.1 Intra-element field

In this approach, the intra-element DEP field $\mathbf{u_e}$ for a particular element e is approximated in terms of a linear combination of fundamental solutions of the problem as

$$\mathbf{u_e} = \mathbf{N_e}\mathbf{c_e} \quad (\mathbf{x} \in \Omega_e, \mathbf{y}_{sj} \notin \Omega_e), \tag{35}$$

where $\mathbf{u_e} = [u_1, u_2, u_3, \phi]^{\mathrm{T}}$, the fundamental solution matrix $\mathbf{N_e}$ and unknown vector $\mathbf{c_e}$ (not nodal displacements) can be written as

$$\mathbf{N_e} = \begin{bmatrix} u_{11}^*(\mathbf{x}, \mathbf{y}_{s1}) & u_{12}^*(\mathbf{x}, \mathbf{y}_{s1}) & u_{13}^*(\mathbf{x}, \mathbf{y}_{s1}) & \dots & u_{11}^*(\mathbf{x}, \mathbf{y}_{sn_s}) & u_{12}^*(\mathbf{x}, \mathbf{y}_{sn_s}) & u_{13}^*(\mathbf{x}, \mathbf{y}_{sn_s}) \\ u_{21}^*(\mathbf{x}, \mathbf{y}_{s1}) & u_{22}^*(\mathbf{x}, \mathbf{y}_{s1}) & u_{23}^*(\mathbf{x}, \mathbf{y}_{s1}) & \dots & u_{21}^*(\mathbf{x}, \mathbf{y}_{sn_s}) & u_{22}^*(\mathbf{x}, \mathbf{y}_{sn_s}) & u_{23}^*(\mathbf{x}, \mathbf{y}_{sn_s}) \\ u_{31}^*(\mathbf{x}, \mathbf{y}_{s1}) & u_{32}^*(\mathbf{x}, \mathbf{y}_{s1}) & u_{33}^*(\mathbf{x}, \mathbf{y}_{s1}) & \dots & u_{31}^*(\mathbf{x}, \mathbf{y}_{sn_s}) & u_{32}^*(\mathbf{x}, \mathbf{y}_{sn_s}) & u_{33}^*(\mathbf{x}, \mathbf{y}_{sn_s}) \\ \phi_{41}^*(\mathbf{x}, \mathbf{y}_{s1}) & \phi_{42}^*(\mathbf{x}, \mathbf{y}_{s1}) & \phi_{43}^*(\mathbf{x}, \mathbf{y}_{s1}) & \dots & \phi_{41}^*(\mathbf{x}, \mathbf{y}_{sn_s}) & \phi_{42}^*(\mathbf{x}, \mathbf{y}_{sn_s}) & \phi_{43}^*(\mathbf{x}, \mathbf{y}_{sn_s}) \end{bmatrix}, \tag{36}$$

$$\mathbf{c_e} = [\,c_{11}\quad c_{21}\quad c_{31}\quad c_{41}\quad \dots\quad c_{1n_s}\quad c_{2n_s}\quad c_{3n_s}\quad c_{4n_s}\,]^{\mathrm{T}}, \tag{37}$$

in which n_s is the number of source points located outside the element domain, and $\mathbf{x}$ and $\mathbf{y}_{sj}$ are, respectively, the field point and source point in the coordinate system (X_1, X_2) local to the element under consideration.

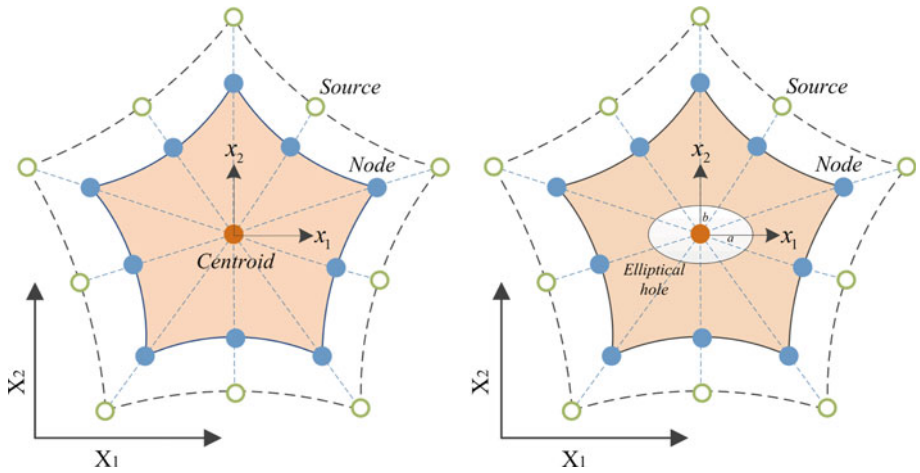

Fig. 3 Intra-element field and frame field of HFS-FEM element for 2D piezoelectric problem: general element (*left*) and special element with central elliptical hole (*right*)

The component $u^*_{ij}(\mathbf{x}, \mathbf{y}_{sj})$ is the induced displacement component ($i = 1, 2, 3$) or electric potential ($i = 4$) in the i-direction at the field point x due to a unit point load ($j = 1,\ 2,\ 3$) or point charge ($j = 4$) applied in the j-direction at the source point $\mathbf{y}_{sj}$. The fundamental solution $u^*_{ij}(\mathbf{x}, \mathbf{y}_{sj})$ is given by Eq. (23) for normal elements or by Eq. (25) for a special elliptical hole element.

In implementation, the number of source points can be taken to be the same as the number of element nodes [27]. The source point $\mathbf{y}_{sj}\,(j = 1, 2, \ldots, n_s)$ is generated by means of the following method in our calculation:

$$\mathbf{y}_s = \mathbf{x}_0 + \gamma(\mathbf{x}_0 - \mathbf{x}_c), \tag{38}$$

where γ is a dimensionless coefficient used to determine the distance between the source point $\mathbf{y}_s$ and the geometrical centroid of the element $\mathbf{x}_c$, and $\mathbf{x}_0$ is a point on the element boundary (the nodal points in this work) as shown in Fig. 3. Determination of γ was discussed in [35], and $\gamma = 5 - 10$ is usually used in practice.

With Eq. (3) and the expression of intra-element DEP field $\mathbf{u}$ in Eq. (35), the corresponding stress and electric displacement Eq. (2) can be further written as

$$\boldsymbol{\sigma} = \mathbf{T_e}\mathbf{c_e}, \tag{39}$$

where $\boldsymbol{\sigma} = \left[\sigma_{11}\ \sigma_{22}\ \sigma_{23}\ \sigma_{31}\ \sigma_{12}\ D_1\ D_2\right]^{\mathrm{T}}$ and

$$\mathbf{T_e} = \begin{bmatrix}
\sigma^*_{11}(\mathbf{x}, \mathbf{y}_{s1}) & \sigma^*_{12}(\mathbf{x}, \mathbf{y}_{s1}) & \sigma^*_{13}(\mathbf{x}, \mathbf{y}_{s1}) & \sigma^*_{14}(\mathbf{x}, \mathbf{y}_{s1}) & \ldots & \sigma^*_{11}(\mathbf{x}, \mathbf{y}_{sn_s}) & \sigma^*_{12}(\mathbf{x}, \mathbf{y}_{sn_s}) & \sigma^*_{13}(\mathbf{x}, \mathbf{y}_{sn_s}) & \sigma^*_{14}(\mathbf{x}, \mathbf{y}_{sn_s}) \\
\sigma^*_{21}(\mathbf{x}, \mathbf{y}_{s1}) & \sigma^*_{22}(\mathbf{x}, \mathbf{y}_{s1}) & \sigma^*_{23}(\mathbf{x}, \mathbf{y}_{s1}) & \sigma^*_{24}(\mathbf{x}, \mathbf{y}_{s1}) & \ldots & \sigma^*_{21}(\mathbf{x}, \mathbf{y}_{sn_s}) & \sigma^*_{22}(\mathbf{x}, \mathbf{y}_{sn_s}) & \sigma^*_{23}(\mathbf{x}, \mathbf{y}_{sn_s}) & \sigma^*_{24}(\mathbf{x}, \mathbf{y}_{sn_s}) \\
\sigma^*_{31}(\mathbf{x}, \mathbf{y}_{s1}) & \sigma^*_{32}(\mathbf{x}, \mathbf{y}_{s1}) & \sigma^*_{33}(\mathbf{x}, \mathbf{y}_{s1}) & \sigma^*_{34}(\mathbf{x}, \mathbf{y}_{s1}) & \ldots & \sigma^*_{31}(\mathbf{x}, \mathbf{y}_{sn_s}) & \sigma^*_{32}(\mathbf{x}, \mathbf{y}_{sn_s}) & \sigma^*_{33}(\mathbf{x}, \mathbf{y}_{sn_s}) & \sigma^*_{34}(\mathbf{x}, \mathbf{y}_{sn_s}) \\
\sigma^*_{41}(\mathbf{x}, \mathbf{y}_{s1}) & \sigma^*_{42}(\mathbf{x}, \mathbf{y}_{s1}) & \sigma^*_{43}(\mathbf{x}, \mathbf{y}_{s1}) & \sigma^*_{44}(\mathbf{x}, \mathbf{y}_{s1}) & \ldots & \sigma^*_{41}(\mathbf{x}, \mathbf{y}_{sn_s}) & \sigma^*_{42}(\mathbf{x}, \mathbf{y}_{sn_s}) & \sigma^*_{43}(\mathbf{x}, \mathbf{y}_{sn_s}) & \sigma^*_{44}(\mathbf{x}, \mathbf{y}_{sn_s}) \\
\sigma^*_{51}(\mathbf{x}, \mathbf{y}_{s1}) & \sigma^*_{52}(\mathbf{x}, \mathbf{y}_{s1}) & \sigma^*_{53}(\mathbf{x}, \mathbf{y}_{s1}) & \sigma^*_{54}(\mathbf{x}, \mathbf{y}_{s1}) & \ldots & \sigma^*_{51}(\mathbf{x}, \mathbf{y}_{sn_s}) & \sigma^*_{52}(\mathbf{x}, \mathbf{y}_{sn_s}) & \sigma^*_{53}(\mathbf{x}, \mathbf{y}_{sn_s}) & \sigma^*_{54}(\mathbf{x}, \mathbf{y}_{sn_s}) \\
\sigma^*_{61}(\mathbf{x}, \mathbf{y}_{s1}) & \sigma^*_{62}(\mathbf{x}, \mathbf{y}_{s1}) & \sigma^*_{63}(\mathbf{x}, \mathbf{y}_{s1}) & \sigma^*_{64}(\mathbf{x}, \mathbf{y}_{s1}) & \ldots & \sigma^*_{61}(\mathbf{x}, \mathbf{y}_{sn_s}) & \sigma^*_{62}(\mathbf{x}, \mathbf{y}_{sn_s}) & \sigma^*_{63}(\mathbf{x}, \mathbf{y}_{sn_s}) & \sigma^*_{64}(\mathbf{x}, \mathbf{y}_{sn_s}) \\
\sigma^*_{71}(\mathbf{x}, \mathbf{y}_{s1}) & \sigma^*_{72}(\mathbf{x}, \mathbf{y}_{s1}) & \sigma^*_{73}(\mathbf{x}, \mathbf{y}_{s1}) & \sigma^*_{74}(\mathbf{x}, \mathbf{y}_{s1}) & \ldots & \sigma^*_{71}(\mathbf{x}, \mathbf{y}_{sn_s}) & \sigma^*_{72}(\mathbf{x}, \mathbf{y}_{sn_s}) & \sigma^*_{73}(\mathbf{x}, \mathbf{y}_{sn_s}) & \sigma^*_{74}(\mathbf{x}, \mathbf{y}_{sn_s})
\end{bmatrix}, \tag{40}$$

in which $\sigma^*_{ij}(\mathbf{x}, \mathbf{y}_{sj})$ denotes the corresponding stress components ($i = 1, 2, 3, 4, 5$) or electric displacement ($i = 6, 7$) along the i-direction at the field point $\mathbf{x}$ due to a unit point load ($j = 1, 2, 3$) or a unit point charge ($j = 4$) applied in the j-direction at the source point $\mathbf{y}_{sj}$. The components $\sigma^*_{ij}(\mathbf{x}, \mathbf{y})$ are given by Eq. (24) when $\hat{\mathbf{p}}_i$ is selected to be $(1, 0, 0, 0)^{\mathrm{T}}$, $(0, 1, 0, 0)^{\mathrm{T}}$, $(0, 0, 1, 0)^{\mathrm{T}}$, and $(0, 0, 0, 1)^{\mathrm{T}}$, respectively. Consequently, the generalized traction forces and electric displacement can be given as

$$\begin{Bmatrix} t_1 \\ t_2 \\ t_3 \\ D_n \end{Bmatrix} = \begin{Bmatrix} \mathbf{Q}_1 \\ \mathbf{Q}_2 \\ \mathbf{Q}_3 \\ \mathbf{Q}_4 \end{Bmatrix} \mathbf{c_e} = \mathbf{Q_e}\mathbf{c_e} \tag{41}$$

where

$$\mathbf{Q_e} = \mathbf{nT_e}, \tag{42}$$

$$\mathbf{n} = \begin{bmatrix} n_1 & 0 & 0 & 0 & n_2 & 0 & 0 \\ 0 & n_2 & 0 & 0 & n_1 & 0 & 0 \\ 0 & 0 & n_2 & n_1 & 0 & 0 & 0 \\ 0 & 0 & 0 & 0 & 0 & n_1 & n_2 \end{bmatrix}. \tag{43}$$

3.1.2 Auxiliary frame field

The unknown $\mathbf{c}_e$ in Eqs. (35) and (41) may be calculated using a hybrid technique [36] in which the intra-element fields of the elements are linked through an auxiliary conforming displacement frame which has the same form as that in the conventional FEM (see Fig. 3). Thus, for the generalized two-dimensional piezoelectric problem under consideration, the frame field is assumed as

$$\tilde{\mathbf{u}}(\mathbf{x}) = \begin{Bmatrix} \tilde{u}_1 \\ \tilde{u}_2 \\ \tilde{u}_3 \\ \tilde{\phi} \end{Bmatrix} = \begin{Bmatrix} \tilde{\mathbf{N}}_1 \\ \tilde{\mathbf{N}}_2 \\ \tilde{\mathbf{N}}_3 \\ \tilde{\mathbf{N}}_4 \end{Bmatrix} \mathbf{d}_e = \tilde{\mathbf{N}}_e \mathbf{d}_e, \quad (\mathbf{x} \in \Gamma_e), \tag{44}$$

where the symbol "$\sim$" is used to specify that the field is defined on the element boundary only, $\mathbf{d}_e = \mathbf{d}_e(\mathbf{c}_e)$ stands for the vector of the nodal displacements which are the final unknowns of the problem, Γ_e represents the boundary of element e, and $\tilde{\mathbf{N}}_e$ is the matrix of shape functions. Taking the side 3-4-5 of a particular 8-node quadrilateral element (see Fig. 3) as an example, $\tilde{\mathbf{N}}_e$ and $\mathbf{d}_e$ can be expressed as

$$\tilde{\mathbf{N}}_e = \begin{bmatrix} 0\cdots0 & \tilde{N}_1 & 0 & 0 & 0 & \tilde{N}_2 & 0 & 0 & 0 & \tilde{N}_3 & 0 & 0 & 0 & 0\cdots0 \\ 0\cdots0 & 0 & \tilde{N}_1 & 0 & 0 & 0 & \tilde{N}_2 & 0 & 0 & 0 & \tilde{N}_3 & 0 & 0 & 0\cdots0 \\ 0\cdots0 & 0 & 0 & \tilde{N}_1 & 0 & 0 & 0 & \tilde{N}_2 & 0 & 0 & 0 & \tilde{N}_3 & 0 & 0\cdots0 \\ \underbrace{0\cdots0}_{8} & 0 & 0 & 0 & \tilde{N}_1 & 0 & 0 & 0 & \tilde{N}_2 & 0 & 0 & 0 & \tilde{N}_3 & \underbrace{0\cdots0}_{12} \end{bmatrix}, \tag{45}$$

$$\mathbf{d_e} = \begin{bmatrix} u_{11} & u_{21} & u_{31} & \phi_1 & \cdots & u_{14} & u_{24} & u_{34} & \phi_4 & \cdots & u_{18} & u_{28} & u_{38} & \phi_8 \end{bmatrix}^{\mathrm{T}}, \tag{46}$$

and $\tilde{N}_1$, $\tilde{N}_2$ and $\tilde{N}_3$ are expressed by the natural coordinate $\xi \in [-1, 1]$

$$\tilde{N}_1 = -\frac{\xi\,(1-\xi)}{2},\ \tilde{N}_2 = 1-\xi^2,\ \tilde{N}_3 = \frac{\xi\,(1+\xi)}{2}\ \ (\xi \in [-1, 1])\,. \tag{47}$$

3.2 Variational principles

Based on the assumption of two distinct DEP fields, the Euler equations of the proposed variational functional should also satisfy the following inter-element continuity requirements in addition to Eqs. (4)–(7):

$$(u_i)_e = (u_i)_f \quad \phi_e = \phi_f \quad (\text{on } \Gamma_e \cap \Gamma_f,\ \text{conformity}), \tag{48}$$

$$(t_i)_e + (t_i)_f = 0 \quad (D_n)_e + (D_n)_f = 0 \quad (\text{on } \Gamma_e \cap \Gamma_f,\ \text{reciprocity}), \tag{49}$$

where "e" and "f" stand for any two neighboring elements. Equations (4)–(7), together with Eqs. (48) and (49), can now be taken as the basis to establish the modified variational principle for constructing the hybrid finite element formulation of the piezoelectric material [23,27].

Since the stationary conditions of the traditional potential or complementary variational functional cannot satisfy the inter-element continuity condition required in the proposed HFS-FEM, a new modified variational functional must be developed. In the absence of the body forces and electric charge density, the hybrid functional Π_{me} for a particular element, say element e, is constructed as

$$\Pi_{me} = \Pi_e + \int_{\Gamma_e} t_i(\tilde{u}_i - u_i)\mathrm{d}\Gamma + \int_{\Gamma_e} D_n(\tilde{\phi} - \phi)\mathrm{d}\Gamma \tag{50}$$

where

$$\Pi_e = \frac{1}{2}\iint\limits_{\Omega_e} (\sigma_{ij}\varepsilon_{ij} + D_i E_i)\mathrm{d}\Omega - \int\limits_{\Gamma_t} \bar{t}_i \tilde{u}_i \mathrm{d}\Gamma - \int\limits_{\Gamma_D} \overline{D}_n \tilde{\phi}\mathrm{d}\Gamma, \tag{51}$$

and the boundary Γ_e of element e is defined as

$$\Gamma_e = \Gamma_{eu} \cup \Gamma_{et} \cup \Gamma_{eI} = \Gamma_{e\phi} \cup \Gamma_{eD} \cup \Gamma_{eI} \tag{52}$$

and

$$\Gamma_{eu} = \Gamma_e \cap \Gamma_u, \Gamma_{et} = \Gamma_e \cap \Gamma_t, \Gamma_{e\phi} = \Gamma_e \cap \Gamma_\phi, \Gamma_{eD} = \Gamma_e \cap \Gamma_D, \tag{53}$$

and Γ_{eI} is the inter-element boundary of element e. Compared to the functional employed in the conventional FEM, the present hybrid functional is constructed by adding two integral terms related to the intra-element and element frame DEP fields to guarantee the satisfaction of displacement and the electrical potential continuity condition on the common boundary of two adjacent elements.

It can be proved that the stationary conditions of the above functional (50) lead to Eqs. (1)–(7). To this end, performing a variation of Π_m, we obtain

$$\delta\Pi_{me} = \delta\Pi_e + \int\limits_{\Gamma_e} [(\tilde{u}_i - u_i)\delta t_i + t_i(\delta\tilde{u}_i - \delta u_i)]\mathrm{d}\Gamma + \int\limits_{\Gamma_e} [(\tilde{\phi} - \phi)\delta D_n + D_n(\delta\tilde{\phi} - \delta\phi)]\mathrm{d}\Gamma, \tag{54}$$

in which the first term is

$$\begin{aligned}\delta\Pi_e &= \iint\limits_{\Omega_e} (\sigma_{ij}\delta\varepsilon_{ij}\mathrm{d}\Omega) + \iint\limits_{\Omega_e} D_i\delta E_i\mathrm{d}\Omega - \int\limits_{\Gamma_{et}} \bar{t}_i\delta\tilde{u}_i\mathrm{d}\Gamma - \int\limits_{\Gamma_{eD}} \overline{D}_n\delta\tilde{\phi}\mathrm{d}\Gamma, \\ &= \iint\limits_{\Omega_e} \sigma_{ij}\delta u_{i,j}\mathrm{d}\Omega + \iint\limits_{\Omega_e} D_i\delta\phi_{,i}\mathrm{d}\Omega - \int\limits_{\Gamma_{et}} \bar{t}_i\delta\tilde{u}_i\mathrm{d}\Gamma - \int\limits_{\Gamma_{eD}} \overline{D}_n\delta\tilde{\phi}\mathrm{d}\Gamma.\end{aligned} \tag{55}$$

Applying Gaussian theorem

$$\iint\limits_{\Omega_e} f_{,i}\mathrm{d}\Omega = \int\limits_{\Gamma_e} f \cdot n_i\mathrm{d}\Gamma, \tag{56}$$

and the definitions of traction force and electrical displacement

$$t_i = \sigma_{ij}n_j, \quad D_n = D_i n_i, \tag{57}$$

and considering the fact that

$$\int\limits_{\Gamma_{eu}} t_i\delta\tilde{u}_i\mathrm{d}\Gamma = 0, \int\limits_{\Gamma_{e\phi}} D_n\delta\tilde{\phi}\mathrm{d}\Gamma = 0, \tag{58}$$

we have

$$\begin{aligned}\delta\Pi_{me} = &- \iint\limits_{\Omega_e} \sigma_{ij,j}\delta u_i\mathrm{d}\Omega - \iint\limits_{\Omega_e} D_{i,i}\delta\phi\mathrm{d}\Omega + \int\limits_{\Gamma_{et}} (t_i - \bar{t}_i)\delta\tilde{u}_i\mathrm{d}\Gamma + \int\limits_{\Gamma_{eD}} (D_n - \overline{D}_n)\delta\tilde{\phi}\mathrm{d}\Gamma \\ &+ \int\limits_{\Gamma_e} (\tilde{u}_i - u_i)\delta t_i\mathrm{d}\Gamma + \int\limits_{\Gamma_e} (\tilde{\phi} - \phi)\delta D_n\mathrm{d}\Gamma + \int\limits_{\Gamma_I} t_i\delta\tilde{u}_i\mathrm{d}\Gamma + \int\limits_{\Gamma_I} D_n\delta\tilde{\phi}\mathrm{d}\Gamma.\end{aligned} \tag{59}$$

Therefore, the Euler equations for Eq. (59) result in Eqs. (1)–(7) and Eq. (48) because the quantities δu_i, δt_i, $\delta\phi$, δD_n, $\delta\tilde{u}_i$, and $\delta\tilde{\phi}$ may be arbitrary.

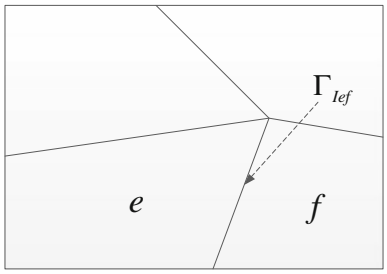

Fig. 4 Illustration of continuity between two adjacent elements "e" and "f"

As for the continuity condition of Eq. (49), it can easily be seen from the following variational of two adjacent elements such as e and f (see Fig. 4) that

$$\begin{aligned}\delta\Pi_{m(e\cup f)} = &-\iint\limits_{\Omega_e\cup\Omega_f}\sigma_{ij,j}\delta u_i \mathrm{d}\Omega - \iint\limits_{\Omega_e\cup\Omega_f} D_{i,i}\delta\phi \mathrm{d}\Omega + \int\limits_{\Gamma_{et}+\Gamma_{et}}(t_i-\bar{t}_i)\delta\tilde{u}_i \mathrm{d}\Gamma + \int\limits_{\Gamma_{eD}+\Gamma_{fD}}(D_n-\overline{D}_n)\delta\tilde{\phi}\mathrm{d}\Gamma \\ &+\int\limits_{\Gamma_e+\Gamma_f}(\tilde{u}_i-u_i)\delta t_i \mathrm{d}\Gamma + \int\limits_{\Gamma_e+\Gamma_f}(\tilde{\phi}-\phi)\delta D_n \mathrm{d}\Gamma + \int\limits_{\Gamma_{efI}}\left(t_{ie}+t_{if}\right)\delta\tilde{u}_i + \int\limits_{\Gamma_{efI}}\left(D_{ne}+D_{nf}\right)\delta\tilde{\phi}\mathrm{d}\Gamma.\end{aligned} \tag{60}$$

This indicates that the stationary condition of the functional satisfies both the required boundary and inter-element continuity equations. Furthermore, the existence of an extremum of functional (50) can be easily proved by the so-called second variational approach, which indicates that functional (50) has a local extreme. Therefore, we can conclude that functional (50) can be used for deriving the hybrid finite element formulation.

3.3 Element stiffness matrix

The element stiffness equation can be generated by setting $\delta\Pi_{me} = 0$. To simplify the derivation, we first transform all domain integrals in Eq. (50) into boundary integrals. Making use of the Gaussian theorem, the functional in Eq. (50) can be simplified as

$$\begin{aligned}\Pi_{me} = &\frac{1}{2}\left(\int\limits_{\Gamma_e} t_i u_i \mathrm{d}\Gamma - \iint\limits_{\Omega_e}\sigma_{ij,j}u_i \mathrm{d}\Omega\right) + \frac{1}{2}\left(\int\limits_{\Gamma_e} D_n\phi \mathrm{d}\Gamma - \iint\limits_{\Omega_e} D_{i,i}\phi \mathrm{d}\Omega\right) - \int\limits_{\Gamma_t}\bar{t}_i\tilde{u}_i \mathrm{d}\Gamma - \int\limits_{\Gamma_D}\overline{D}_n\tilde{\phi}\mathrm{d}\Gamma \\ &+\int\limits_{\Gamma_e} t_i(\tilde{u}_i-u_i)\mathrm{d}\Gamma + \int\limits_{\Gamma_e} D_n(\tilde{\phi}-\phi)\mathrm{d}\Gamma.\end{aligned} \tag{61}$$

Due to satisfaction of the equilibrium equation with the constructed intra-element fields, we have the following expression for the HFS-FEM:

$$\Pi_{me} = -\frac{1}{2}\int\limits_{\Gamma_e}(t_i u_i + D_n\phi)\mathrm{d}\Gamma + \int\limits_{\Gamma_e}(t_i\tilde{u}_i + D_n\tilde{\phi})\mathrm{d}\Gamma - \int\limits_{\Gamma_t}\bar{t}_i\tilde{u}_i\mathrm{d}\Gamma - \int\limits_{\Gamma_D}\overline{D}_n\tilde{\phi}\mathrm{d}\Gamma. \tag{62}$$

Substituting Eqs. (35), (41), and (44) into the functional (62) yields the formulation

$$\Pi_{me} = -\frac{1}{2}\mathbf{c}_e^{\mathrm{T}}\mathbf{H}_e\mathbf{c}_e + \mathbf{c}_e^{\mathrm{T}}\mathbf{G}_e\mathbf{d}_e - \mathbf{d}_e^{\mathrm{T}}\mathbf{g}_e \tag{63}$$

where

$$\mathbf{H}_e = \int\limits_{\Gamma_e}\mathbf{Q}_e^{\mathrm{T}}\mathbf{N}_e\mathrm{d}\Gamma, \quad \mathbf{G}_e = \int\limits_{\Gamma_e}\mathbf{Q}_e^{\mathrm{T}}\tilde{\mathbf{N}}_e\mathrm{d}\Gamma, \quad \mathbf{g}_e = \int\limits_{\Gamma_t}\tilde{\mathbf{N}}_e^{\mathrm{T}}\bar{\mathbf{t}}\mathrm{d}\Gamma + \int\limits_{\Gamma_D}\tilde{\mathbf{N}}_e^{\mathrm{T}}\overline{\mathbf{D}}\mathrm{d}\Gamma. \tag{64}$$

To enforce inter-element continuity on the common element boundary, the unknown vector $\mathbf{c}_e$ should be expressed in terms of nodal DOF $\mathbf{d}_e$. The stationary condition of the functional Π_{me} with respect to $\mathbf{c}_e$ and $\mathbf{d}_e$, respectively, yields

$$\frac{\partial \Pi_{me}}{\partial \mathbf{c}_e^{\mathrm{T}}} = -\mathbf{H}_e\mathbf{c}_e + \mathbf{G}_e\mathbf{d}_e = \mathbf{0}, \quad \frac{\partial \Pi_{me}}{\partial \mathbf{d}_e^{\mathrm{T}}} = \mathbf{G}_e^{\mathrm{T}}\mathbf{c}_e - \mathbf{g}_e = \mathbf{0}, \tag{65}$$

from which the relationship between $\mathbf{c}_e$ and $\mathbf{d}_e$ and the stiffness equation can be obtained,

$$\mathbf{c}_e = \mathbf{H}_e^{-1}\mathbf{G}_e\mathbf{d}_e, \tag{66}$$

$$\mathbf{K}_e\mathbf{d}_e = \mathbf{g}_e, \tag{67}$$

where $\mathbf{K}_e = \mathbf{G}_e^{\mathbf{T}}\mathbf{H}_e^{-1}\mathbf{G}_e$ is the element stiffness matrix.

Following the procedure given in [27], the missing rigid-body motion can be recovered by setting the augmented internal field of a particular element e as

$$\mathbf{u}_e = \mathbf{N}_e\mathbf{c}_e + \begin{bmatrix} 1 & 0 & 0 & 0 & 0 & -x_2 & 0 \\ 0 & 1 & 0 & 0 & 0 & x_1 & 0 \\ 0 & 0 & 1 & x_2 & -x_1 & 0 & 0 \\ 0 & 0 & 0 & 0 & 0 & 0 & 1 \end{bmatrix}\mathbf{c}_0, \tag{68}$$

where the undetermined rigid-body motion parameter $\mathbf{c}_0$ can be calculated using the least square matching of $\mathbf{u_e}$ and $\tilde{\mathbf{u}}_\mathbf{e}$ at element nodes,

$$\min = \sum_{i=1}^{n}\left[(u_{1i} - \tilde{u}_{1i})^2 + (u_{2i} - \tilde{u}_{2i})^2 + (u_{3i} - \tilde{u}_{3i})^2 + (\phi_i - \tilde{\phi}_i)^2\right], \tag{69}$$

which finally gives

$$\mathbf{c_0} = \mathbf{R}_e^{-1}\mathbf{r_e}, \tag{70}$$

$$\mathbf{R_e} = \sum_{i=1}^{n}\begin{bmatrix} 1 & 0 & 0 & 0 & 0 & -x_{2i} & 0 \\ 0 & 1 & 0 & 0 & 0 & x_{1i} & 0 \\ 0 & 0 & 1 & x_{2i} & -x_{1i} & 0 & 0 \\ 0 & 0 & x_{2i} & x_{2i}^2 & -x_{1i}x_{2i} & 0 & 0 \\ 0 & 0 & -x_{1i} & -x_{1i}x_{2i} & x_{1i}^2 & 0 & 0 \\ -x_{2i} & x_{1i} & 0 & 0 & 0 & x_{1i}^2 + x_{2i}^2 & 0 \\ 0 & 0 & 0 & 0 & 0 & 0 & 1 \end{bmatrix}, \tag{71}$$

$$\mathbf{r_e} = \sum_{i=1}^{n}\begin{Bmatrix} \Delta u_{e1i} \\ \Delta u_{e2i} \\ \Delta u_{e3i} \\ \Delta u_{e3i}x_{2i} \\ -\Delta u_{e3i}x_{1i} \\ \Delta u_{e2i}x_{1i} - \Delta u_{e1i}x_{2i} \\ \Delta\phi_{ei} \end{Bmatrix}, \tag{72}$$

in which $\mathbf{\Delta u}_{ei} = (\tilde{\mathbf{u}}_e - \hat{\mathbf{u}}_e)|_{\mathbf{node i}}$ and n is the number of element nodes. As a consequence, $\mathbf{c}_0$ can be calculated by Eq. (70) once the nodal DEP fields $\mathbf{d}_e$ and the interpolation coefficients $\mathbf{c}_e$ are, respectively, determined by Eqs. (67) and (66). Then, the complete DEP fields $\mathbf{u}_e$ can be obtained from Eq. (68).

3.4 Normalization of the variables

The orders of magnitude of the material constants and the corresponding field variables in piezoelectricity have a wide spectrum, as large as 10^{19} in SI units. This will lead to an ill-conditioned matrix of the system. To resolve this problem, normalization of each quantity by its reference value should be employed in dealing with piezoelectric problems. The reference values for the stiffness, piezoelectric stress constant, dielectric constants, and strain are selected to be $c_0 = 10^{11}(\mathrm{N/m^2})$, $e_0 = 10^{1}(\mathrm{N/mV})$, $k_0 = 10^{-9}(\mathrm{C/mV})$, $\varepsilon_0 = 10^{-3}(\mathrm{V/m})$, respectively. The reference values of other quantities, as shown in Table 1, are determined in terms of these four fundamental reference variables and the characteristic length $x_0 = 10^{0}(m)$ of the problem, so that the normalized governing equations remain in exactly the same form as the original equations.

Table 1 Reference values for material constants and field variables in piezoelectricity derived from basic reference variables: c_0, e_0, k_0, ε_0 and x_0

Displacement	$u_0 = x_0\varepsilon_0 = 10^{-3}$ (m)	Electric potential	$\phi_0 = x_0 E_0 = 10^7$ (V)
Stress	$\sigma_0 = c_0\varepsilon_0 = 10^8$ (N/m^2)	Electric induction	$D_0 = k_0 E_0 = 10^{-2}$ (C/m^2)
Compliance	$s_0 = \frac{\varepsilon_0}{\sigma_0} = 10^{-11}$ (m^2/N)	Impermeability	$\beta_0 = \frac{E_0}{D_0} = 10^9$ (mV/C)
Electric field	$E_0 = \frac{\sigma_0}{e_0} = 10^7$ (V/m)	Piezoelectric strain constant	$g_0 = \frac{E_0}{\sigma_0} = 10^{-1}$ (mV/N)

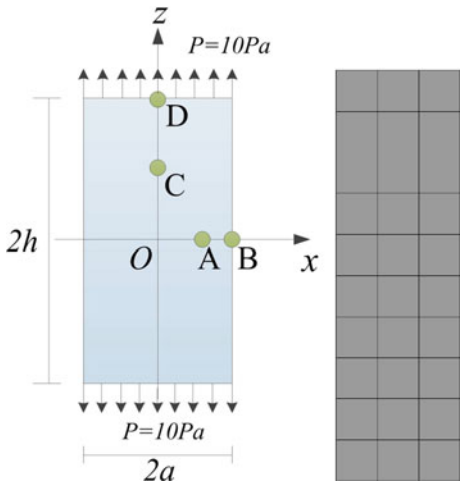

Fig. 5 Geometry, boundary conditions, and mesh configuration of the piezoelectric prism

4 Numerical examples

Several numerical examples are presented in this section to illustrate the application of the HFS-FEM and to demonstrate its effectiveness and accuracy.

4.1 Simple tension of a piezoelectric prism

In this example, a PZT-4 piezoelectric prism subjected to simple tension, as shown in Fig. 8, is investigated by the proposed HFS-FEM. The properties of the material PZT-4 are as follows [37]:

$$
\begin{aligned}
&c_{11} = 12.6 \times 10^{10}\ \text{Nm}^{-2}, c_{12} = 7.78 \times 10^{10}\ \text{Nm}^{-2}, c_{13} = 7.43 \times 10^{10}\ \text{Nm}^{-2},\\
&c_{33} = 11.5 \times 10^{10}\ \text{Nm}^{-2}, c_{44} = 2.56 \times 10^{10}\ \text{Nm}^{-2},\\
&e_{15} = 12.7\ \text{Cm}^{-2}, e_{31} = -5.2\ \text{Cm}^{-2}, e_{33} = 15.1\ \text{Cm}^{-2},\\
&\kappa_{11} = 730\kappa_0, \kappa_{33} = 635\kappa_0, \kappa_0 = 8.854 \times 10^{-12}\ \text{C/Nm}.
\end{aligned}
$$

In this analysis, the dimensions of the geometry are set to be $a = 3$ m, $h = 10$ m, $P = 10$ Pa. Considering the symmetry conditions of the problem, only one quadrant of the prism is modeled by HFS-FEM. The corresponding boundary conditions are

$$
\begin{aligned}
&\sigma_{xx} = \sigma_{xz} = D_x = 0 && \text{at } x = \pm a,\\
&\sigma_{zz} = P,\ \ \sigma_{xz} = D_z = 0 && \text{at } z = \pm h.
\end{aligned}
$$

As shown in Fig. 5, 30 quadrilateral elements are used in this model. The displacements and electric potential of the four selected reference points: A (2,0), B (3,0), C (0,5), and D (0,10) are listed in Table 2. The analytical results of the corresponding points are also given for comparison [37]. It can be seen that the HFS-FEM results are in good agreement with the analytical ones. The contour plots of the piezoelectric plate under simple tension are given in Fig. 6, clearly demonstrating that the displacement field and electrical distribution are in linear variation as expected.

Table 2 Comparison of the predicted results by HFS-FEM with the analytical results

Position	$u_x(10^{-10}\,\mathrm{m})$	$u_z(10^{-9}\,\mathrm{m})$	$\phi(\mathrm{V})$	$\sigma_{xx}(\mathrm{N\,m^{-2}})$	$\sigma_{zz}(\mathrm{N\,m^{-2}})$	$D_z(\mathrm{N\,m^{-2}})$
A	−0.7220	0.0000	0.0000	0.0018	9.9991	−0.0000
	(−0.7222)	(0.0000)	(0.0000)	(0.0000)	(10.000)	(0.0000)
B	−1.0831	0.0000	0.0000	0.0019	9.9992	−0.0003
	(−1.0834)	(0.0000)	(0.0000)	(0.0000)	(10.000)	(0.0000)
C	0.0000	0.3914	1.2187	0.0018	9.9992	−0.0000
	(0.0000)	(0.3915)	(1.2183)	(0.0000)	(10.000)	(0.0000)
D	0.0000	0.7828	2.4373	0.0019	9.9991	−0.0001
	(0.0000)	(0.7829)	(2.4367)	(0.0000)	(10.000)	(0.0000)

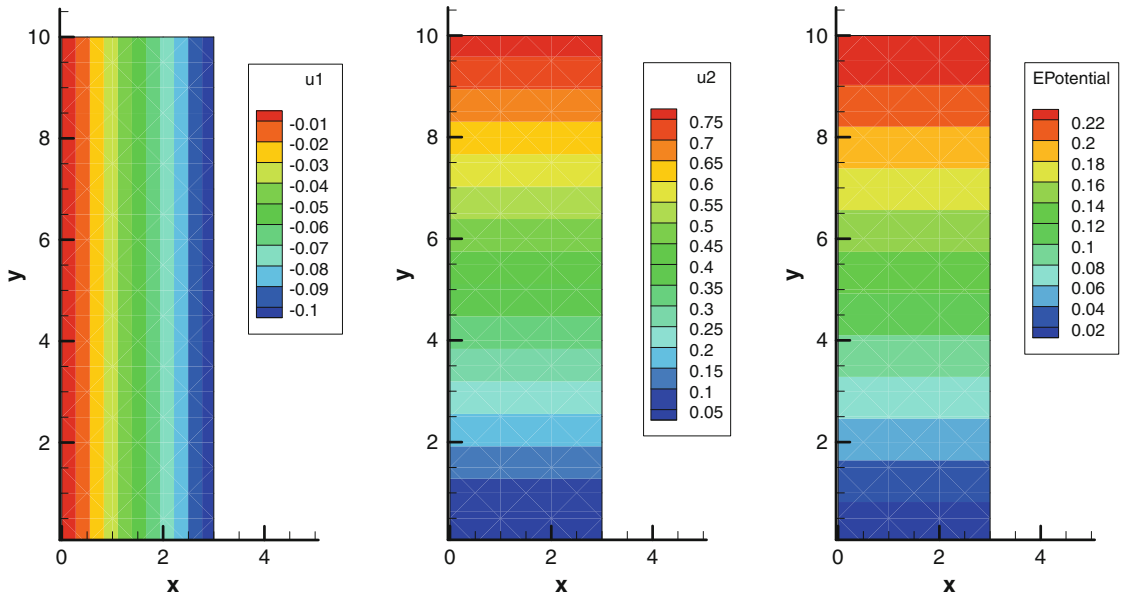

Fig. 6 Contour plot of the displacement and electric potential of the plate

4.2 Infinite piezoelectric plate with a circular hole

In this example, an infinite piezoelectric plate with a circular hole as shown in Fig. 7 is assessed by the new HFS-FEM. The material parameters used are given in Table 3. We suppose that a remote mechanical load $\sigma_{zz}^{\infty} = \sigma_0$ or electrical load $D_{zz}^{\infty} = D_0$ is applied to the plate along the z axis direction (poling direction), while traction- and electric-charge-free boundary conditions are applied on the edge of the hole. According to our previous study, we assume the radius of the hole to be $r = 1$ and $L/r = 20$, to approximate the infinite piezoelectric plate in this work. In our analysis, 117 eight-node quadratic elements are employed for the quarter piezoelectric plate. The results for the stress σ_θ and electric displacement D_θ are normalized with respect to either the far field applied stress $\sigma_{zz}^{\infty} = \sigma_0$ or the far field applied electric displacement $D_{zz}^{\infty} = D_0$.

Figure 8 presents the variations of the normalized stress σ_θ/σ_0 and the normalized electric displacement $D_\theta/\sigma_0 \times 10^{10}$ along the hole edge under remote mechanical load. Clearly, the results obtained from the HFS-FEM agree very well with those from the analytical solution by Sosa [4]. It is also verified that when the loading is in the poling direction, the electromechanical coupling effect can alleviate the stress concentration occurring in the plate. It can be observed from Fig. 8 that the maximum values of σ_θ appear at $\theta = 0°$ and $\theta = 180°$ for the applied load σ_{zz}^{∞}, which also agrees well with the analytical solution from Sosa [4]. Figure 9 shows that the maximum values of D_θ appear at $\theta = 65°$ and $\theta = 115°$, which also agrees well with the analytical solution from Sosa.

Figure 10 shows the variation of normalized stress $\sigma_\theta/D_0 \times 10^8$ and electrical displacement D_θ/D_0 along the hole boundary under remote electrical load. It can be seen from Fig. 10 that the electric displacement can induce marked stress concentration problems in piezoelectric materials with defects, up to $\sigma_\theta/D_0 \times 10^8$ times the applied D_0. It can be seen from Fig. 11 that D_θ reaches its maximum at $\theta = 0°$ and its minimum at $\theta = 180°$, which also agrees well with the analytical solution from Sosa [5]. To achieve the same accuracy,

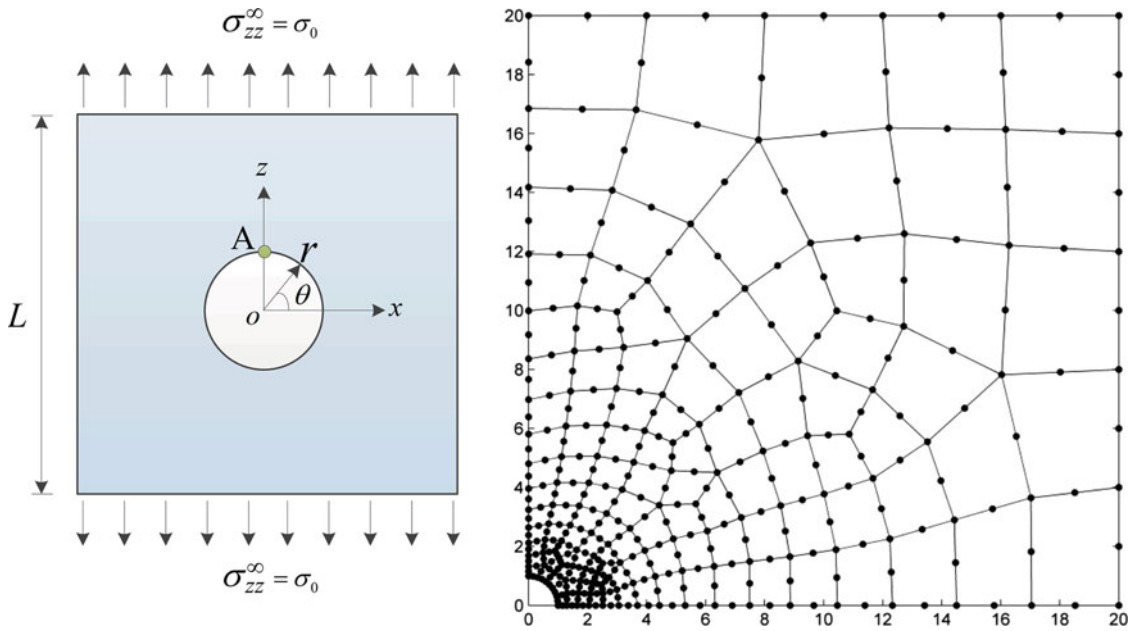

Fig. 7 An infinite piezoelectric plate with a circular hole subjected to remote stress

Table 3 Properties of the material PZT-4 used in Example 1

Parameters	Values	Parameters	Values
c_{11}	$13.9 \times 10^{10}\,\mathrm{N\,m^{-2}}$	e_{15}	$13.44\,\mathrm{C\,m^{-2}}$
c_{12}	$7.78 \times 10^{10}\,\mathrm{N\,m^{-2}}$	e_{31}	$-6.98\,\mathrm{C\,m^{-2}}$
c_{13}	$7.43 \times 10^{10}\,\mathrm{N\,m^{-2}}$	e_{33}	$13.84\,\mathrm{C\,m^{-2}}$
c_{33}	$11.3 \times 10^{10}\,\mathrm{N\,m^{-2}}$	κ_{11}	$6.0 \times 10^{-9}\,\mathrm{C/N\,m}$
c_{44}	$2.56 \times 10^{10}\,\mathrm{N\,m^{-2}}$	κ_{33}	$5.47 \times 10^{-9}\,\mathrm{C/N\,m}$

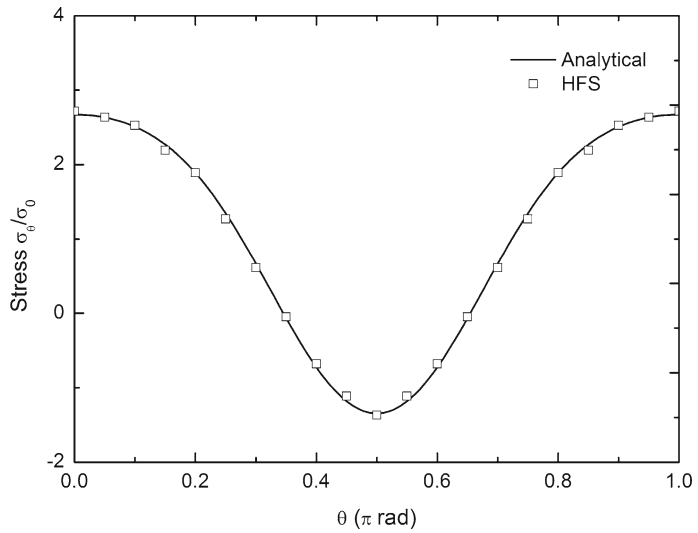

Fig. 8 Variation of normalized stress σ_θ/σ_0 along the hole boundary under remote mechanical load

960 eight-node ordinary parametric elements are needed to model a quarter of the plate [38]. It is obvious that the computational efficiency of HFS-FEM is superior for this case. Figure 12 shows the contour plots of stress and electric displacement components around the elliptical hole in the piezoelectric plate when applying a remote mechanical load along z direction.

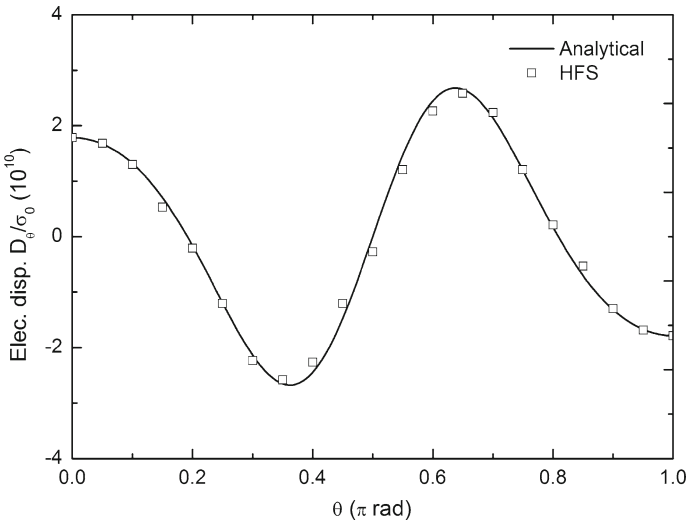

Fig. 9 Variation of normalized electrical displacement $D_\theta/\sigma_0 \times 10^{10}$ along the hole boundary under remote mechanical load

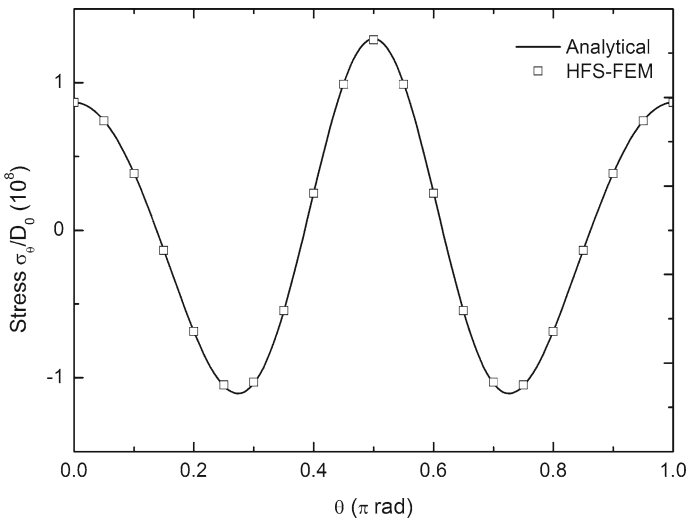

Fig. 10 Variation of normalized stress $\sigma_\theta/D_0 \times 10^8$ along the hole boundary under remote electrical load

4.3 Infinite piezoelectric plate with elliptical hole

To investigate the performance of the special element, an infinite piezoelectric plate containing an elliptical hole is modeled by the HFS-FEM. A uniform remote tension σ_0 is applied in the z direction. The material parameters are the same as those used in Example 4.2. In our analysis, as shown in Fig. 13, the infinite plate is approximated by a finite domain with the length and width assumed to be $L = W = 20$ mm, and the geometry of the ellipse is $a = 2b = 2$ mm. In this case, it is not necessary to use numerous elements to capture the concentrated stress as in the traditional FEM. A relatively coarse mesh can be employed, and the elliptical hole can be analyzed by only one special element. There are 49 elements in all, with a total of 176 nodes: 48 eight-node conventional hybrid elements and one central special element containing the elliptical hole, as shown in Fig. 14.

Figure 15 shows the variations of the normalized hoop stress σ_θ/σ_0 and electric displacement D_θ/σ_0 along the rim of the elliptical hole. It can be seen from Fig. 15 that the results obtained from the HFS-FEM are in very good agreement with the analytical solutions. This indicates that the proposed method with a special element can capture the dramatic variations of hoop stress and electric displacement induced by the elliptical hole in the plate. Compared with the traditional FEM, the HFS-FEM method with special element has the capability

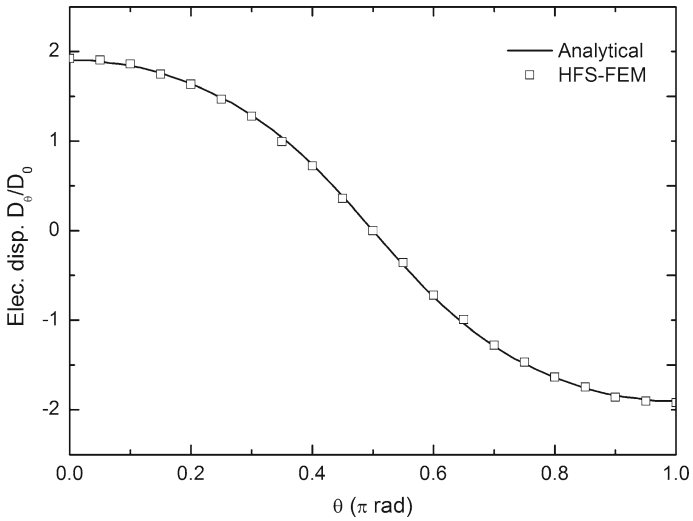

Fig. 11 Variation of normalized electrical displacement D_θ / D_0 along the hole boundary under remote electrical load

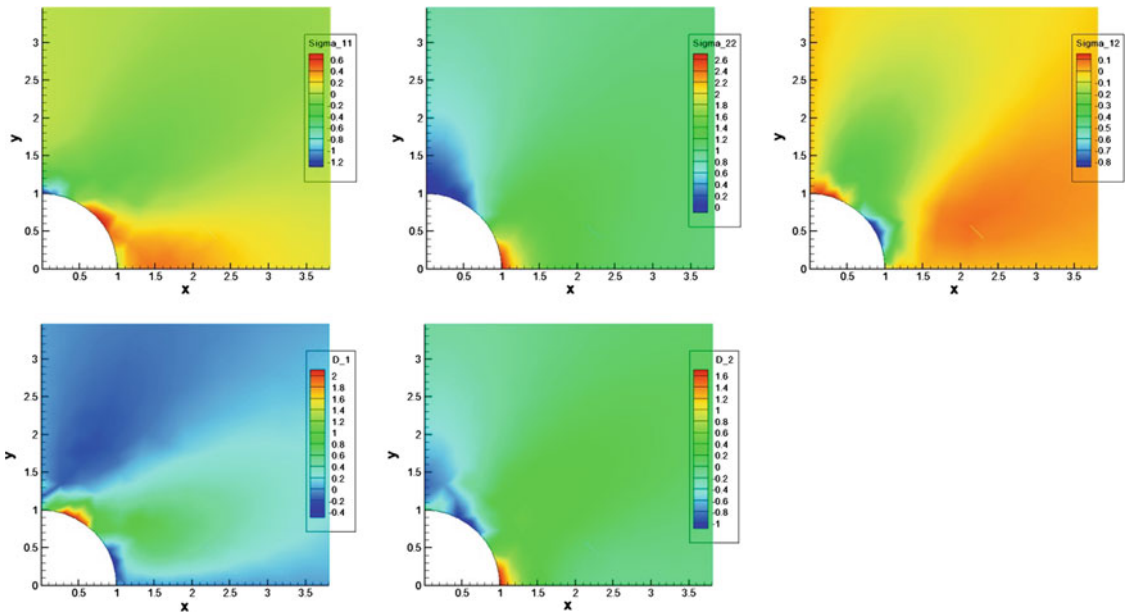

Fig. 12 Contour plots of stress and electric displacement components around the elliptic hole in the piezoelectric plate under remote mechanical load

to use much less elements to capture the stress concentration incurred by the defects and will greatly reduce the computation effort in piezoelectric analysis.

4.4 An infinite piezoelectric plate with a center crack

In this example, the extreme case of an elliptical hole is considered. By letting the minor axis b equal zero, an elliptical hole can be made into a crack of length $2a$. The geometry and loading for this problem are shown in Fig. 16. The dimensions are assumed to be $2a/W = 0.1$ and $L/W = 1$, so that it can be approximated to an infinite plate with a finite crack. The plate is made of PZT-5H ceramic, and the material parameters are listed in Table 4. The remote mechanical loading and electric loading are $\sigma_{zz}^{\infty} = 1.0 \times 10^6$ Pa, $\sigma_{zx}^{\infty} = 1.0 \times 10^6$ Pa and $D_{zz}^{\infty} = 1.0 \times 10^6$ C/m^2. The same mesh as used in Example 4.3 is employed for this problem. The stress and electric intensity factors K_I, K_{II} and K_{IV} calculated by the proposed HFS-FEM are given in Table 5, in

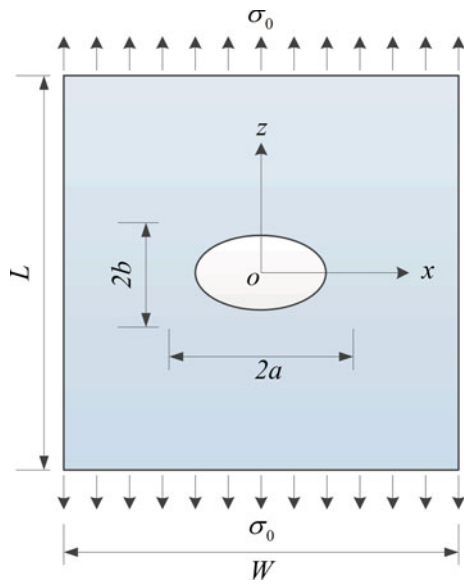

Fig. 13 Schematic of an infinite piezoelectric plate with an elliptic hole under remote tension

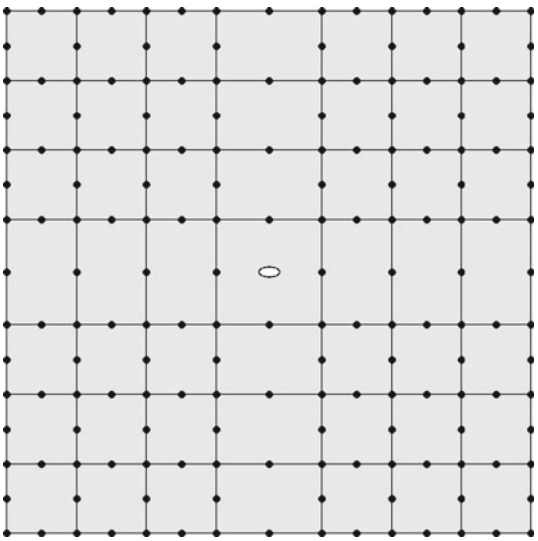

Fig. 14 Mesh configuration with special element for the piezoelectric plate

Table 4 Properties of the material PZT-5H used in Example 4

Parameters	Values	Parameters	Values
c_{11}	$12.6 \times 10^{10}\,\mathrm{N\,m^{-2}}$	e_{15}	$17.0\,\mathrm{C\,m^{-2}}$
c_{12}	$5.5 \times 10^{10}\,\mathrm{N\,m^{-2}}$	e_{31}	$-6.5\,\mathrm{C\,m^{-2}}$
c_{13}	$5.3 \times 10^{10}\,\mathrm{N\,m^{-2}}$	e_{33}	$23.3\,\mathrm{C\,m^{-2}}$
c_{33}	$11.7 \times 10^{10}\,\mathrm{N\,m^{-2}}$	κ_{11}	$15.1 \times 10^{-9}\,\mathrm{C/N\,m}$
c_{44}	$3.53 \times 10^{10}\,\mathrm{N\,m^{-2}}$	κ_{33}	$13.0 \times 10^{-9}\,\mathrm{C/N\,m}$

which the analytical solutions obtained from the formulations of Sosa and the BEM results [4,37] are listed for comparison. Figure 17 shows the variation of K_{IV} with respect to the applied remote electric displacement D_{zz}^{∞}. It can be seen from Table 5 and Fig. 17 that the results from the HFS-FEM exhibit good agreement with the analytical solutions, and the accuracy is similar to that of the BEM.

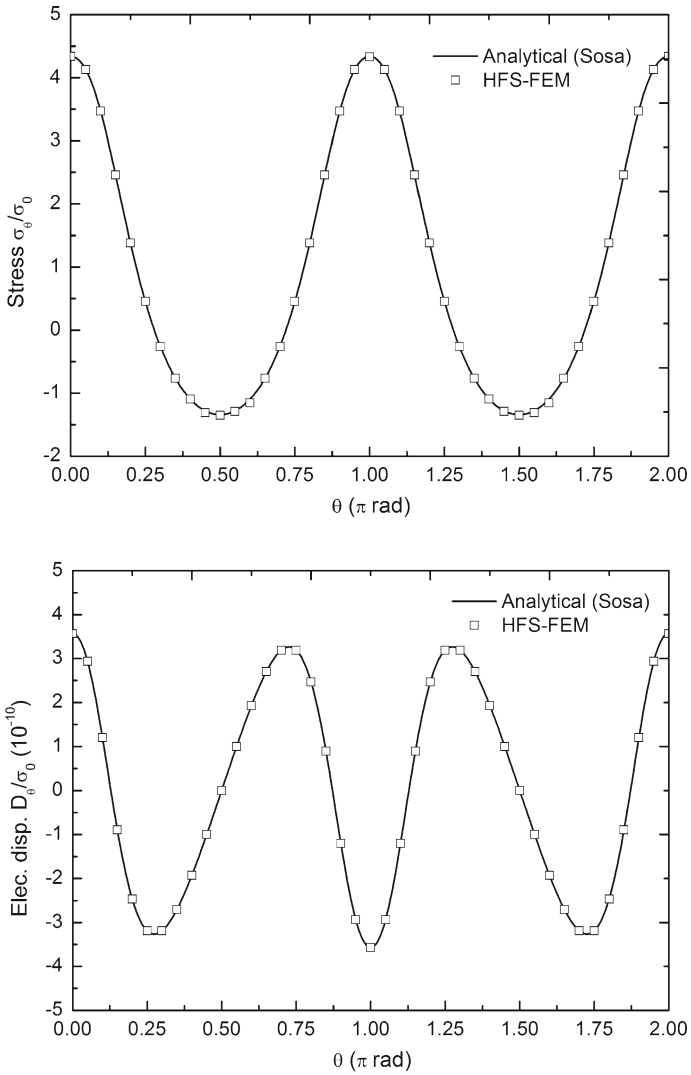

Fig. 15 Variations of the normalized hoop stress σ_θ/σ_0 and electric displacement D_θ/σ_0 along the rim of the elliptical hole

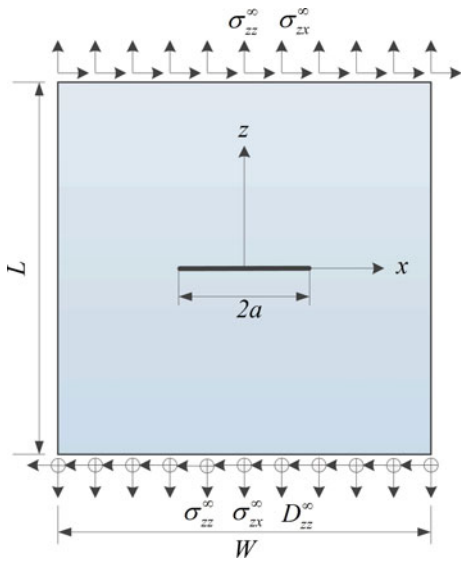

Fig. 16 An orthotropic plate with a center crack under uniform tension

Table 5 The stress and electric intensity factors K_{I}, K_{II} and K_{IV}

Method	$K_{\mathrm{I}}(10^6\,\mathrm{N\,m^{-3/2}})$	$K_{\mathrm{II}}(10^6\,\mathrm{N\,m^{-3/2}})$	$K_{\mathrm{IV}}(10^{-3}\,\mathrm{N\,m^{-3/2}})$
HFS-FEM	0.1761	0.1707	0.1753
BEM	0.1757	0.1708	0.1750
Analytical	0.1772	0.1772	0.1772

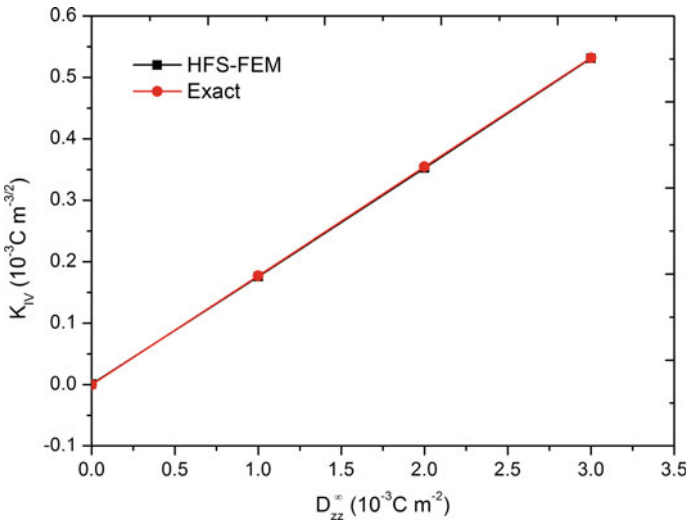

Fig. 17 The variation of K_{IV} with respect to the applied remote electric displacement D_{zz}^{∞}

5 Conclusions

Based on the fundamental solutions derived from the elegant Stroh formalism, a new efficient hybrid finite element scheme HFS-FEM is developed for modeling plane piezoelectric materials with defects. In this method, the general or special fundamental solutions of the piezoelectric materials are employed to approximate the intra-element DEP, and the element frame field is interpolated by common shape functions. The element stiffness matrix is derived from the modified variational functional, whose minimization conditions lead to boundary conditions and continuity conditions between any two adjacent elements. To verify and evaluate the performance of the new method, four numerical examples are considered, and the results from HFS-FEM are compared with those from analytical solutions or the literature. It is demonstrated that the HFS-FEM has good performance in the analysis of the coupling behavior of piezoelectric materials under various loading conditions. The special element is able to capture the strong stress/electric displacement concentration around the elliptical hole and can obtain accurate stress intensity factors for cracks while simultaneously avoiding the need for very fine meshing around such defects. The HFS-FEM offers the attractive possibility of developing accurate crack singular, corner, or perforated elements, simply by using appropriate special fundamental solutions as the trial functions of the intra-element displacements. It is concluded that HFS-FEM is a promising numerical method for solving complex engineering problems.

Acknowledgments C.C. would like to thank Professor Chyanbin Hwu and Mr. Shenghan Ho from National Cheng Kung University for helpful discussions on Stroh formalism.

References

1. Barsoum, R.G.S.: Active materials and adaptive structures. Smart Mater. Struct. **6**, 117–122 (1997)
2. Park, S.B., Park, S.S., Carman, G.P., Hahn, H.T.: Measuring strain distribution during mesoscopic domain reorientation in a ferroelectric material. Trans. ASME J. Eng. Mater. Technol. **120**, 1–6 (1998)
3. Cao, C., Qin, Q.H., Yu, A.: Hybrid fundamental-solution-based FEM for piezoelectric materials. Comput. Mech. **50**, 397–412 (2012)
4. Qin, Q.H., Mai, Y.W., Yu, S.W.: Some problems in plane thermopiezoelectric materials with holes. Int. J. Solids Struct. **36**, 427–439 (1999)

5. Park, S., Sun, C.: Effect of electric field on fracture of piezoelectric ceramics. Int. J. Fract. **70**, 203–216 (1993)
6. Qin, Q.H., Mai, Y.W.: Crack growth prediction of an inclined crack in a half-plane thermopiezoelectric solid. Theor. Appl. Fract. Mech. **26**, 185–191 (1997)
7. Qin, Q.H.: Solving anti-plane problems of piezoelectric materials by the Trefftz finite element approach. Comput. Mech. **31**, 461–468 (2003)
8. Sheng, H., Wang, H., Ye, J.: State space solution for thick laminated piezoelectric plates with clamped and electric open-circuited boundary conditions. Int. J. Mech. Sci. **49**, 806–818 (2007)
9. Willberg, C., Gabbert, U.: Development of a three-dimensional piezoelectric isogeometric finite element for smart structure applications. Acta Mech. **223**, 1837–1850 (2012)
10. Xiao, Z.M., Yan, J., Chen, B.J.: Electro-elastic stress analysis for a Zener-Stroh crack interacting with a coated inclusion in a piezoelectric solid. Acta Mech. **171**, 29–40 (2004)
11. Qin, Q.H., Lu, M.: BEM for crack-inclusion problems of plane thermopiezoelectric solids. Int. J. Numer. Methods Eng. **48**, 1071–1088 (2000)
12. Jański, Ł., Scherzer, M., Steinhorst, P., Kuna, M.: Adaptive finite element computation of dielectric and mechanical intensity factors in piezoelectrics with impermeable cracks. Int. J. Numer. Methods Eng. **81**, 1492–1513 (2010)
13. Yu, P., Guo, W., She, C., Zhao, J.: The influence of Poisson's ratio on thickness-dependent stress concentration at elliptic holes in elastic plates. Int. J. Fatigue **30**, 165–171 (2008)
14. Lee, J.S., Jiang, L.Z.: A boundary integral formulation and 2D fundamental solution for piezoelastic media. Mech. Res. Commun. **21**, 47–54 (1994)
15. Pan, E.: A BEM analysis of fracture mechanics in 2D anisotropic piezoelectric solids. Eng. Anal. Bound. Elem. **23**, 67–76 (1999)
16. Xu, X.L., Rajapakse, R.K.N.D.: On a plane crack in piezoelectric solids. Int. J. Solids Struct. **38**, 7643–7658 (2001)
17. Sheng, N., Sze, K.Y., Cheung, Y.K.: Trefftz solutions for piezoelectricity by Lekhnitskii's formalism and boundary-collocation method. Int. J. Numer. Methods Eng. **65**, 2113–2138 (2006)
18. Ting, T.C.T.: Anisotropic Elasticity: Theory and Applications. Oxford Science Publications, New York (1996)
19. Qin, Q.H., Mai, Y.W.: BEM for crack-hole problems in thermopiezoelectric materials. Eng. Fract. Mech., **69**, 577–588 (2002)
20. Hwu, C., Yen, W.J.: Green's functions of two-dimensional anisotropic plates containing an elliptic hole. Int. J. Solids Struct. **27**, 1705–1719 (1991)
21. Qin, Q.H.: Hybrid-Trefftz finite-element method for Reissner plates on an elastic-foundation. Comput. Methods Appl. Mech. Eng. **122**, 379–392 (1995)
22. Sze, K.Y., Liu, G.H., Fan, H.: Four- and eight-node hybrid-Trefftz quadrilateral finite element models for Helmholtz problem. Comput. Methods Appl. Mech. Eng. **199**, 598–614 (2010)
23. Qin, Q.H.: Variational formulations for TFEM of piezoelectricity. Int. J. Solids Struct. **40**, 6335–6346 (2003)
24. Qin, Q.H.: Hybrid Trefftz finite-element approach for plate-bending on an elastic-foundation. Appl. Math. Model. **18**, 334–339 (1994)
25. Piltner, R.: Special finite elements with holes and internal cracks. Int. J. Numer. Methods Eng. **21**, 1471–1485 (1985)
26. Dhanasekar, M., Han, J., Qin, Q.H.: A hybrid-Trefftz element containing an elliptic hole. Finite Elem. Anal. Des. **42**, 1314–1323 (2006)
27. Qin, Q.H., Wang, H.: Matlab and C Programming for Trefftz Finite Element Methods. CRC Press, New York (2008)
28. Wang, H., Qin, Q.H.: Fundamental-solution-based finite element model for plane orthotropic elastic bodies. Eur. J. Mech. A Solids **29**, 801–809 (2010)
29. Cao, C., Yu, A., Qin, Q.H.: Evaluation of effective thermal conductivity of fiber-reinforced composites. Int. J. Archit. Eng. Const. **1**, 14–29 (2012)
30. Cao, C., Qin, Q.H., Yu, A.: A new hybrid finite element approach for three-dimensional elastic problems. Arch. Mech. **64**, 261–292 (2012)
31. Wang, H., Qin, Q.H.: A new special element for stress concentration analysis of a plate with elliptical holes. Acta Mech. **223**, 1323–1340 (2012)
32. Stroh, A.N.: Dislocations and cracks in anisotropic elasticity. Phil. Mag. **3**, 625–639 (1958)
33. Lu, P., Williams, F.: Green functions of piezoelectric material with an elliptic hole or inclusion. Int. J. Solids Struct. **35**, 651–664 (1998)
34. Suo, Z., Kuo, C.M., Barnett, D.M., Willis, J.R.: Fracture mechanics for piezoelectric ceramics. J. Mech. Phys. Solids **40**, 739–765 (1992)
35. Wang, H., Qin, Q.H., Kang, Y.L.: A new meshless method for steady-state heat conduction problems in anisotropic and inhomogeneous media. Arch. Appl. Mech. **74**, 563–579 (2005)
36. Wang, H., Qin, Q.H.: Hybrid FEM with fundamental solutions as trial functions for heat conduction simulation. Acta Mech. Solida Sin. **22**, 487–498 (2009)
37. Ding, H.J., Wang, G.Q., Chen, W.Q.: A boundary integral formulation and 2D fundamental solutions for piezoelectric media. Comput. Methods Appl. Mech. Eng. **158**, 65–80 (1998)
38. Deng, Q., Wang, Z.: Analysis of piezoelectric materials with an elliptical hole. Acta Mech. Sin. **34**, 109–114 (2002)